Optimal single concave sliding device properties for isolated multi-span continuous deck bridges depending on the ground motion characteristics

Soil Dynamics and Earthquake Engineering 173 (2023) 108128

Contents lists available at ScienceDirect

Soil Dynamics and Earthquake Engineering

journal homepage: www.elsevier.com/locate/soildyn

Optimal single concave sliding device properties for isolated multi-span continuous deck bridges depending on the ground motion characteristics

Paolo Castaldo, Elena Miceli *

Department of Structural, Geotechnical and Building Engineering (DISEG), Politecnico di Torino, Turin, Italy

ARTICLE INFO

Keywords:
Multi-span continuous deck bridges
Seismic isolation
Non-dimensional equations
Seismic performance
Optimal friction coefficient
PGA/PGV ratio

ABSTRACT

The present study investigates the analysis of the optimal friction coefficient with respect to the seismic performance of isolated multi-span continuous deck bridges, equipped with single concave friction pendulum (FPS) isolators. A six-degree-of-freedom system is used to model the structural system and the FPS friction property is described by means of a law that considers the dependency on the velocity. The equations of motions have been implemented in nondimensional form by considering the peak ground acceleration-to-velocity ratio (*PGA/PGV*) and the peak ground acceleration (*PGA*) as ground motion parameters for two different sets of seismic records: near-fault and far-field inputs. In addition, different bridge models are considered for various parameters (i.e., pier period, deck period, friction coefficient and mass of the structural system). The results show the effectiveness of the *PGA/PGV* ratio within the proposed nondimensionalization together with the existence of an optimum value of the friction coefficient that minimizes the nondimensional response of the pier. At the end, a linear regression expression is presented with the aim to compute the optimal value of the normalized friction coefficient as a function of the deck period and *PGA/PGV* ratio, which can be used in the preliminary phase to design the FPS bearings. Additionally, a multivariate non-linear regression expression is also provided to evaluate the pier response.

1. Introduction

Currently, one of the most effective solutions to enhance the seismic performance of bridges is the adoption of the isolation technique. The main effect of this strategy is to reduce the seismic inertia forces acting on the deck and thus transmitted to the substructure, by increasing the period of the isolation system [1–3]. Among the possible isolation devices (e.g., high or low damping elastomeric bearings, lead-rubber bearings, sliding bearings) [4–6], the friction pendulum system (FPS) bearings have the important advantages of both decoupling the isolation period from the deck mass and dissipating energy thanks to the friction between the concave surface and slider [7–9]. Many researches have investigated the behaviour of the FPS isolators through both experimental and numerical analyses [10–20]. In detail, the improvement of the seismic performance of a three-span continuous deck highway bridge, adopting double concave friction pendulum devices, is commented in Ref. [21]. In Ref. [22], different mathematical models are studied to represent the response of bridges under real earthquake ground motions, demonstrating the accuracy of the results when simplified approaches are adopted to model the flexibility of the piers and of the deck. An experimental test on a 1:6 scale railway bridge isolated with friction pendulum bearings is described in Ref. [23] using a shake table, with the goal to study the influence of transverse poundings on the seismic response. Three-dimensional models of multi-span steel girder bridges isolated with FPS devices are investigated in Ref. [24], by changing many modeling parameters (i.e., geometrical and material characteristics of the bridge and isolator design properties). The effectiveness of variable friction pendulum system for a three-span continuous deck bridge under near-fault ground motions is analyzed in Ref. [25]. Seismic reliability-based abacuses for the design of FPS devices have been proposed in Ref. [26] for multi-span continuous deck bridges.

Contextually, Jangid [27,28] observed the existence of an optimal value for the friction coefficient in isolators able to minimize the structural response under seismic events, including respectively stochastic random processes and near-fault ground motions as seismic inputs. Successively, other works have been focused on this issue proposing non-dimensional analyses of different structural systems as a

* Corresponding author.
E-mail addresses: paolo.castaldo@polito.it, pcastaldo@unisa.it (P. Castaldo), elena.miceli@polito.it (E. Miceli).

https://doi.org/10.1016/j.soildyn.2023.108128
Received 13 March 2023; Received in revised form 3 June 2023; Accepted 11 July 2023

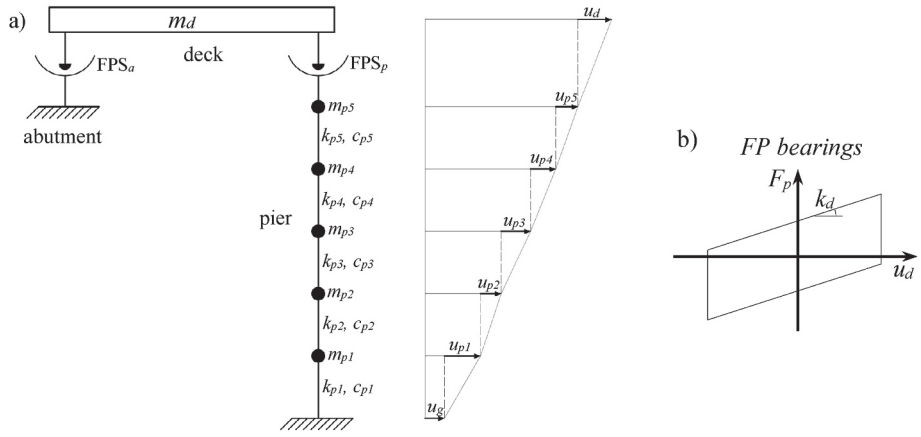

Fig. 1. 6dof model of a multi-span continuous deck bridge isolated by FPS devices (a); response of the FPS device on the pier (b).

function of the most relevant parameters. Specifically, the research of [29] considered the influence of the seismic input intensity and the soil condition on the optimal friction coefficient for isolated piers. Non-dimentionalizations with respect to the seismic input intensity for multi-span continuous deck bridges isolated with single and double concave FPS devices have been proposed, respectively, by Refs. [30,31]. Similarly, in Ref. [32] it was performed a normalization of the time of the seismic input with respect to its harmonic frequency omega, to evaluate the dynamics of the sliding response of structures.The frequency content of the ground motions in terms of *PGA/PGV* ratio has been considered to assess the optimal properties of the FPS isolators for base-isolated buildings in Ref. [33]. The *PGA/PGV* ratio has been also adopted by Refs. [34–36] to investigate the relation between the optimal isolator properties and the ground motion inputs for seismically isolated bridges.

This work examines the seismic performance of multi-span continuous composite or reinforced concrete (RC) deck bridges isolated with single concave FPS devices. The aim is to evaluate the influence of ground motion characteristics on the optimal friction coefficient of the isolators by means of a non-dimensionalization of the motion equations. In agreement with [15,22,30,31], a six-degree-of-freedom (dof) model has been adopted, including 5 dofs for the lumped masses of the RC pier and 1 additional dof for the composite or RC deck, which is considered infinitely rigid. Two FPS devices are modelled, respectively, on top of the elastic RC pier and on the rigid RC abutment. The latter is modelled as a fixed support in order to include the interaction between the deck and the abutment. The velocity dependency of the FPS device behavior is taken into account according to Ref. [10]. To include the record-to-record variability, different sets of ground motions are considered, including both far-field (FF) records with different ranges of peak ground acceleration-to-velocity ratios (i.e., *PGA/PGV*) and near-fault (NF) inputs [33]. By including the *PGA/PGV* ratio, the non-dimensionalization of the motion equations with respect to the seismic intensity has been proposed. In addition, a wide parametric analysis is implemented (i.e., the pier period, the ratio between the deck period and the period associated to the ground motion input, the friction coefficient and the ratio between the mass of the deck and of the pier). In this way, the normalized responses in terms of peak horizontal displacement of the pier and of the isolators are assessed. Finally, a linear regression expression is evaluated in order to compute the normalized friction coefficient of the isolators with respect to the ratio between the deck period and the ground motion period. This proposed expression can be very useful for a preliminary design of the FPS devices to isolate multi-span continuous composite or RC deck bridges. Additionally, a multivariate non-linear regression expression is also provided to evaluate the seismic pier response.

2. Non-dimensional analysis for multi-span continuous desk bridges isolated with FPS devices

To model the response of multi-span continuous composite or RC deck bridges isolated with single concave FPS devices, a 6-dof system is implemented, according to Refs. [15,22,30,31]. Specifically, 5 dofs are adopted for the elastic RC pier and 1 additional dof for the rigid composite or RC deck (Fig. 1(a)). The choice of discretizing the pier in 5 lumped masses is a trade-off between the computational effort and the accuracy in the assessment of the corresponding elastic response, as commented in Ref. [30]. Two FPS devices are placed, respectively, on top of the rigid and fixed RC abutment and on top of the pier, as shown in Fig. 1(a). In agreement with [15,22,30,31], it is underlined that the presence of non-structural elements such as parapets or kerbs are not modelled. In addition, the effects of soil-structure interaction [7,37,38] as well as the combination of horizontal and vertical components of ground motions or the asynchronous effects [3,20,38–40] are not included in the present study. It should also be underlined that this model is representative of multi-span continuous deck bridges having spans of similar length and piers with similar stiffness. The analysis can be effective also for piers with different heights depending on the effects due to the higher modes.

The dimensional equations of motion for the 6-dof system under a seismic input $\ddot{u}_g(t)$ along the longitudinal direction are:

$$m_d\ddot{u}_d(t)+m_d\ddot{u}_{p5}(t)+m_d\ddot{u}_{p4}(t)+m_d\ddot{u}_{p3}(t)+m_d\ddot{u}_{p2}(t)+m_d\ddot{u}_{p1}(t)+c_d\dot{u}_d(t)+F_p(t)+F_a(t)=-m_d\ddot{u}_g(t) \tag{1a}$$

$$m_{p5}\ddot{u}_{p5}(t)+m_{p5}\ddot{u}_{p4}(t)+m_{p5}\ddot{u}_{p3}(t)+m_{p5}\ddot{u}_{p2}(t)+m_{p5}\ddot{u}_{p1}(t)-c_d\dot{u}_d(t)+c_{p5}\dot{u}_{p5}(t)+k_{p5}u_{p5}(t)-F_p(t)=-m_{p5}\ddot{u}_g(t) \tag{1b}$$

$$m_{p4}\ddot{u}_{p4}(t)+m_{p4}\ddot{u}_{p3}(t)+m_{p4}\ddot{u}_{p2}(t)+m_{p4}\ddot{u}_{p1}(t)-c_{p5}\dot{u}_{p5}(t)-k_{p5}u_{p5}(t)+c_{p4}\dot{u}_{p4}(t)+k_{p4}u_{p4}(t)=-m_{p4}\ddot{u}_g(t) \tag{1c}$$

$$m_{p3}\ddot{u}_{p3}(t)+m_{p3}\ddot{u}_{p2}(t)+m_{p3}\ddot{u}_{p1}(t)-c_{p4}\dot{u}_{p4}(t)-k_{p4}u_{p4}(t)+c_{p3}\dot{u}_{p3}(t)+k_{p3}u_{p3}(t)=-m_{p3}\ddot{u}_g(t) \tag{1d}$$

$$m_{p2}\ddot{u}_{p2}(t)+m_{p2}\ddot{u}_{p1}(t)-c_{p3}\dot{u}_{p3}(t)-k_{p3}u_{p3}(t)+c_{p2}\dot{u}_{p2}(t)+k_{p2}u_{p2}(t)=-m_{p2}\ddot{u}_g(t) \tag{1e}$$

$$m_{p1}\ddot{u}_{p1}(t) - c_{p2}\dot{u}_{p2}(t) - k_{p2}u_{p2}(t) + c_{p1}\dot{u}_{p1}(t) + k_{p1}u_{p1}(t) = -m_{p1}\ddot{u}_g(t) \quad (1f)$$

where u_d represents the horizontal displacement of the deck relative to the pier top, u_{pi} is the displacement of the i-th lumped mass of the pier with respect to the subsequently inferior one, m_d is the deck mass, m_{pi} and k_{pi} are, respectively, the mass and stiffness of the i-th dof of the pier, assumed equal for all the dofs, c_{pi} is the inherent viscous damping coefficient of each dof of the pier, c_d is the viscous coefficient of the bearing, t is the time instant, the dot indicates differentiation over time, while $F_a(t)$ and $F_p(t)$ are the resisting forces of the FPS devices placed on top of the abutment and of the pier, respectively, expressed as [8]:

$$F_a(t) = \frac{m_d g}{2}\left[\frac{1}{R_a}\left(u_d(t) + \sum_{i=1}^{5} u_{pi}\right) + \mu_a\left(\dot{u}_d + \sum_{i=1}^{5}\dot{u}_{pi}\right)\mathrm{sgn}\left(\dot{u}_d + \sum_{i=1}^{5}\dot{u}_{pi}\right)\right] \quad (2a)$$

$$F_p(t) = \frac{m_d g}{2}\left[\frac{1}{R_p}u_d(t) + \mu_p(\dot{u}_d)\mathrm{sgn}(\dot{u}_d)\right] \quad (2b)$$

The first part of both Eq.s(2a,b) indicates the elastic component of the force while the second addendum is the friction one (Fig. 1(b)). In detail, $k_d = W/R = m_d g/(2R)$, g is the gravity constant, R represents the radius of curvature of the FPS bearing on the abutment (i.e., R_a) or on the pier (i.e., R_p), μ denotes the sliding friction coefficient for the FPS bearing on the abutment (i.e., μ_a) or on the pier (i.e., μ_p). The difference between Eq. (2a) and Eq. (2b) is that $F_a(t)$ depends on the displacement and velocity of the deck with respect to the ground while the force on the pier $F_p(t)$ is a function of the relative displacement and velocity of the deck with respect to the pier top. According to the experimental results [8,10,14,16], the sliding friction coefficient of teflon-steel interfaces is velocity-dependent and can be expressed as:

$$\mu(\dot{u}) = f_{\max} - (f_{\max} - f_{\min})\cdot\exp(-\alpha|\dot{u}|) \quad (3)$$

where $\dot{u} = \dot{u}_d$ in case of μ_p or $\dot{u} = \dot{u}_d + \sum_{i=1}^{5}\dot{u}_{pi}$ in case of μ_a, $f_{\max}$ and $f_{\min}$ are the sliding coefficients at large and zero velocity respectively, α is the parameter that controls the transition from low to large velocities. According to Refs. [16,31–33], it can be assumed $f_{\max} = 3f_{\min}$ with $\alpha = 30$.

Eq.s(1a-f) are based on the assumptions of equal FPS isolators with low curvatures: $f_{\max} = f_{\max,a} = f_{\max,b}$ and $f_{\min} = f_{\min,a} = f_{\min,b}$ as well as $R{=}R_a = R_p$. Therefore, the fundamental period of the isolated bridge is $T_d = 2\pi\sqrt{m_d/(2k_d)} = 2\pi\sqrt{R/g}$, which does not depend on the mass of the bridge but only on the radius of curvature of the isolating device [8].

In this study, it is proposed a non-dimensional analysis following the approaches of [30–33] inspired by Refs. [41,42]. In detail, according to Buckingham's Π-theorem [43,44], it is possible to normalize the dimensional terms of Eq.s(1a-f) by means of time-scale and length-scale factors. In the following, the time scale is assumed as $1/\omega_g$, where $\omega_g = 2\pi/T_g$ is herein assumed as representative circular frequency of the ground motion and, in a simplified way, calculated as the ratio between the peak ground acceleration and velocity (i.e., $\omega_g = PGA/PGV$), while the length scale is assumed as a_0/ω_g^2, where a_0 is an acceleration measuring the seismic intensity. Thus, the seismic input can be expressed as:

$$\ddot{u}_g(t) = a_0 l(t) = a_0 \ell(\tau) \quad (4)$$

where $l(t)$ is a nondimensional function describing the variation of the seismic input over time, while $\ell(\tau)$ is obtained from $l(t)$ by means of the time scale, such that $\tau = t\omega_g$. By dividing Eq.s(1a-f) by the deck mass m_d and introducing both the time and length scale factors, the nondimensional equations become:

$$\ddot{\psi}_d(\tau) + \ddot{\psi}_{p5}(\tau) + \ddot{\psi}_{p4}(\tau) + \ddot{\psi}_{p3}(\tau) + \ddot{\psi}_{p2}(\tau) + \ddot{\psi}_{p1}(\tau) + 2\xi_d\frac{\omega_d}{\omega_g}\dot{\psi}_d(\tau) + \left[\frac{1}{2}\frac{\omega_d^2}{\omega_g^2}\psi_d(\tau) + \frac{\mu_p(\dot{u}_d)g}{2a_0}\mathrm{sgn}(\dot{\psi}_d)\right] + \\ + \left[\frac{1}{2}\frac{\omega_d^2}{\omega_g^2}\left(\psi_d(\tau) + \sum\nolimits_{i=1}^{5}\psi_{pi}(\tau)\right) + \frac{g}{2a_0}\mu_a\left(\dot{u}_d + \sum_{i=1}^{5}\dot{u}_{pi}\right)\left(\mathrm{sgn}\left(\dot{\psi}_d + \sum_{i=1}^{5}\dot{\psi}_{pi}\right)\right)\right] = -\ell(\tau) \quad (5a)$$

$$\lambda_{p5}\left[\ddot{\psi}_{p5}(\tau) + \ddot{\psi}_{p4}(\tau) + \ddot{\psi}_{p3}(\tau) + \ddot{\psi}_{p2}(\tau) + \ddot{\psi}_{p1}(\tau)\right] - 2\xi_d\frac{\omega_d}{\omega_g}\dot{\psi}_d(\tau) + 2\xi_{p5}\frac{\omega_{p5}}{\omega_g}\lambda_{p5}\dot{\psi}_{p5}(\tau) + \\ + \lambda_{p5}\frac{\omega_{p5}^2}{\omega_g^2}\psi_{p5}(\tau) - \left[\frac{1}{2}\frac{\omega_d^2}{\omega_g^2}\psi_d(\tau) + \frac{\mu_p(\dot{\psi}_d)g}{2a_0}\mathrm{sgn}(\dot{\psi}_d)\right] = -\lambda_{p5}\ell(\tau) \quad (5b)$$

$$\lambda_{p4}\left[\ddot{\psi}_{p4}(\tau) + \ddot{\psi}_{p3}(\tau) + \ddot{\psi}_{p2}(\tau) + \ddot{\psi}_{p1}(\tau)\right] - 2\xi_{p5}\frac{\omega_{p5}}{\omega_g}\lambda_{p5}\dot{\psi}_{p5}(\tau) + 2\xi_{p4}\frac{\omega_{p4}}{\omega_g}\lambda_{p4}\dot{\psi}_{p4}(\tau) - \lambda_{p5}\frac{\omega_{p5}^2}{\omega_g^2}\psi_{p5}(\tau) + \lambda_{p4}\frac{\omega_{p4}^2}{\omega_g^2}\psi_{p4}(\tau) = -\lambda_{p4}\ell(\tau) \quad (5c)$$

$$\lambda_{p3}\left[\ddot{\psi}_{p3}(\tau) + \ddot{\psi}_{p2}(\tau) + \ddot{\psi}_{p1}(\tau)\right] - 2\xi_{p4}\frac{\omega_{p4}}{\omega_g}\lambda_{p4}\dot{\psi}_{p4}(\tau) + 2\xi_{p3}\frac{\omega_{p3}}{\omega_g}\lambda_{p3}\dot{\psi}_{p3}(\tau) - \lambda_{p4}\frac{\omega_{p4}^2}{\omega_g^2}\psi_{p4}(\tau) + \lambda_{p3}\frac{\omega_{p3}^2}{\omega_g^2}\psi_{p3}(\tau) = -\lambda_{p3}\ell(\tau) \quad (5d)$$

$$\lambda_{p2}\left[\ddot{\psi}_{p2}(\tau) + \ddot{\psi}_{p1}(\tau)\right] - 2\xi_{p3}\frac{\omega_{p3}}{\omega_g}\lambda_{p3}\dot{\psi}_{p3}(\tau) + 2\xi_{p2}\frac{\omega_{p2}}{\omega_g}\lambda_{p2}\dot{\psi}_{p2}(\tau) - \lambda_{p3}\frac{\omega_{p3}^2}{\omega_g^2}\psi_{p3}(\tau) + \lambda_{p2}\frac{\omega_{p2}^2}{\omega_g^2}\psi_{p2}(\tau) = -\lambda_{p2}\ell(\tau) \quad (5e)$$

$$\lambda_{p1}\ddot{\psi}_{p1}(\tau) - 2\xi_{p2}\frac{\omega_{p2}}{\omega_g}\lambda_{p2}\dot{\psi}_{p2}(\tau) + 2\xi_{p1}\frac{\omega_{p1}}{\omega_g}\lambda_{p1}\dot{\psi}_{p1}(\tau) - \lambda_{p2}\frac{\omega_{p2}^2}{\omega_g^2}\psi_{p2}(\tau) \\ + \lambda_{p1}\frac{\omega_{p1}^2}{\omega_g^2}\psi_{p1}(\tau) \\ = -\lambda_{p1}\ell(\tau) \quad (5f)$$

where $\psi_d = \frac{u_d\omega_g^2}{a_0}$ and $\psi_{pi} = \frac{u_{pi}\omega_g^2}{a_0}$ are the normalized displacements of the deck and of the i-th lumped mass of the pier, respectively, $\omega_d = \sqrt{k_d/m_d}$ and $\omega_{pi} = \sqrt{k_{pi}/m_{pi}}$ are the circular vibration frequencies of the isolated deck and of the i-th dof of the pier, respectively, $\xi_d = c_d/2m_d\omega_d$ and $\xi_{pi} = c_{pi}/2m_{pi}\omega_{pi}$ are the damping factors of the isolated deck and of the i-th dof of the pier, respectively, and $\lambda_p = \lambda_{pi} = m_{pi}/m_d$ is the mass ratio

Table 1
Subset of far-field records corresponding to high PGA/PGV values [PGA(g)/PGV>1.2 s/m].

Earthquake	Date	M	Site	Epic. Dist. (km)	Comp.	PGA (g)	PGV (m/s)	PGA(g)/PGV (s/m)	Soil
Parkfield California	June 27, 1966	5.6	Temblor No. 2	7	N65W	0.269	0.145	1.86	Rock
Parkfield California	June 27, 1966	5.6	Cholame, Shandon No. 5	5	N85W	0.434	0.255	1.70	Rock
San Francisco California	Mar. 22, 1957	5.25	Golden Gate Park	11	S80E	0.105	0.046	2.28	Rock
San Francisco California	Mar. 22, 1957	5.25	State Bldg., S.F.	17	S09E	0.085	0.051	1.67	Stiff Soil
Helena Montana	Oct. 31, 1935	6	Carroll College	8	N00E	0.146	0.072	2.03	Rock
Lytle Creek	Sep. 12, 1970	5.4	Wrightwood, California	15	S25W	0.198	0.096	2.06	Rock
Oroville California	Aug. 1, 1975	5.7	Seismogr. StationOroville	13	N53W	0.084	0.044	1.91	Rock
San Fernando California	Feb. 9, 1971	6.4	Pacomia Dam	4	S74W	1.075	0.577	1.86	Rock
San Fernando California	Feb. 9, 1971	6.4	Lake Hughes, Station 4	26	S21W	0.146	0.085	1.72	Rock
NahanniN.W.T., Canada	Dec. 23, 1985	6.9	Site 1, Iverson	7.5	LONG	1.101	0.462	2.38	Rock
Central Honshu Japan	Feb. 26, 1971	5.5	Yoneyama Bridge	27	TRANS	0.151	0.059	2.56	Stiff Soil
Near E. Coast of Honshu Japan	May. 11, 1972	5.8	Kushiro CentralWharf	33	N00E	0.146	0.060	2.43	Stiff Soil
Honshu Japan	Apr. 5, 1966	5.4	Hoshina–A	4	N00E	0.270	0.111	2.43	Stiff Soil
Monte Negro Yugoslavia	Apr. 9, 1979	5.4	Albatros Hotel, Ulcinj	12.5	N00E	0.042	0.016	2.63	Rock
Banja Luka Yugoslavia	Aug. 13, 1981	6.1	Seism. Station, Banja Luka	8.5	N90W	0.074	0.032	2.31	Rock

Table 2
Subset of far-field records corresponding to medium PGA(g)/PGV values [0.8 s/m < PGA(g)/PGV<1.2 s/m].

Earthquake	Date	M	Site	Epic. Dist. (km)	Comp.	PGA (g)	PGV (m/s)	PGA(g)/ PGV (s/m)	Soil
Imperial Valley California	May 18, 1940	6.6	El Centro	8	S00E	0.348	0.334	1.04	Stiff Soil
Kern County California	July 21, 1952	7.6	Taft Lincoln School Tunnel	56	S69E	0.179	0.177	1.01	Rock
Kern County California	July 21, 1952	7.6	Taft Lincoln School Tunnel	56	N21E	0.156	0.157	0.99	Rock
Borrego Mtn. California	April 8, 1968	6.5	San Onofre SCE Power Plant	122	N57W	0.046	0.042	1.10	Stiff Soil
Borrego Mtn. California	April 8, 1968	6.5	San Onofre SCE Power Plant	122	N33E	0.041	0.037	1.11	Stiff Soil
San Fernando California	Feb. 9, 1971	6.4	3838 Lankershim Blvd., L.A.	24	S90W	0.150	0.149	1.01	Rock
San Fernando California	Feb. 9, 1971	6.4	Hollywood Storage P.E. Lot, L.A.	35	N90E	0.211	0.211	1.00	Stiff Soil
San Fernando California	Feb. 9, 1971	6.4	3407 6th Street, L.A.	39	N90E	0.165	0.166	0.99	Stiff Soil
San Fernando California	Feb. 9, 1971	6.4	Griffith Park Observatory, L.A.	31	S00W	0.180	0.205	0.88	Rock
San Fernando California	Feb. 9, 1971	6.4	234 Figueroa St., L.A.	41	N37E	0.199	0.167	1.19	Stiff Soil
Near E. Coast of Honshu, Japan	Nov. 16, 1974	6.1	Kashima Harbor Works	38	N00E	0.07	0.072	0.97	Stiff Soil
Near E. Coast of Honshu, Japan	Aug. 2, 1971	7	Kushiro Central Wharf	196	N90E	0.078	0.068	1.15	Stiff Soil
Monte Negro Yugoslavia	Apr. 15, 1979	7	Albatros Hotel, Ulcinj	17	N00E	0.171	0.194	0.88	Rock
Mexico Earthq.	Sept. 19 1985	8.1	El Suchil, Guerrero Array	230	S00E	0.105	0.116	0.91	Rock
Mexico Earthq.	Sept. 19 1985	8.1	La Villita, Guerrero Array	44	N90E	0.123	0.105	1.17	Rock

Table 3
Subset of far-field records corresponding to low PGA(g)/PGV values [PGA(g)/PGV<0.8 s/m].

Earthquake	Date	M	Site	Epic. Dist. (km)	Comp.	PGA (g)	PGV (m/s)	PGA(g)/ PGV (s/m)	Soil
Long Beach California	Mar. 10, 1933	6.3	Subway Terminal, L.A.	59	N51W	0.097	0.237	0.41	Rock
Long Beach California	Mar. 10, 1933	6.3	Subway Terminal, L.A.	59	N39E	0.064	0.173	0.37	Rock
Lower Calif.	Dec. 30, 1934	6.5	El Centro	58	S00W	0.160	0.209	0.77	Stiff Soil
San Fernando California	Feb. 9, 1971	6.4	2500 Wilshire Blvd., L.A.	40	N61W	0.101	0.193	0.52	Stiff Soil
San Fernando California	Feb. 9, 1971	6.4	3550 Wilshire Blvd., L.A.	39	WEST	0.132	0.216	0.61	Stiff Soil
San Fernando California	Feb. 9, 1971	6.4	222 Figueroa St., L.A.	41	S37W	0.129	0.186	0.69	Stiff Soil
San Fernando California	Feb. 9, 1971	6.4	3470 WilshireBlvd., L.A.	39	S90W	0.114	0.186	0.61	Stiff Soil
San Fernando California	Feb. 9, 1971	6.4	4680 WilshireBlvd., L.A.	38	N15E	0.117	0.215	0.54	Stiff Soil
San Fernando California	Feb. 9, 1971	6.4	445 Figueroa St., L.A.	41	S38W	0.119	0.173	0.69	Rock
San Fernando California	Feb. 9, 1971	6.4	Hollywood Storage L.A.	32	S00W	0.106	0.170	0.62	Stiff Soil
Near E. Coast of Honshu, Japan	May 16, 1968	7.9	Muroran Harbor	290	N00E	0.226	0.334	0.68	Stiff Soil
Near E. Coast of Honshu, Japan	June 17, 1973	7.4	Kushiro Central Wharf	112	N00E	0.205	0.275	0.75	Stiff Soil
Mexico Earthq.	Sep. 19, 1985	8.1	Zihuatenejo, Guerrero Array	135	S00E	0.103	0.159	0.65	Rock
Mexico Earthq.	Sep. 19, 1985	8.1	Teacalco, Cuerrero Array	333	N00E	0.052	0.074	0.70	Rock
Mexico Earthq.	Sep. 19, 1985	8.1	Mesa VibradoraC.U., Mexico City	379	N90W	0.040	0.110	0.36	Rock

corresponding to the *i*-th lumped mass (where all the lumped masses are assumed equal). It follows that the nondimensional or normalized parameters of the problem, denoted as Π variables, are:

$$\Pi_{\omega_p} = \frac{\omega_p}{\omega_d}, \Pi_{\omega_g} = \frac{\omega_d}{\omega_g}, \Pi_\lambda = \lambda_p, \Pi_{\xi_d} = \xi_d, \Pi_{\xi_p} = \xi_{pi},$$
$$\Pi_{\mu,a} = \frac{\mu_a\left(\ddot{u}_d + \sum_{i=1}^{5}\ddot{u}_{pi}\right)g}{a_0}, \Pi_{\mu,p} = \frac{\mu_p(\ddot{u}_d)g}{a_0} \quad (6a, b, c, d, e, f, g)$$

where the first term measures the degree of isolation, while the second one indicates the ratio between the circular frequency of the isolated system and *PGA/PGV*. The terms $\Pi_\lambda = \lambda_p, \Pi_{\xi_d} = \xi_d, \Pi_{\xi_p} = \xi_{pi}$ have been previously explained. The last two terms $\Pi_{\mu,a}$ and $\Pi_{\mu,p}$ represent the normalized friction coefficients. It is worth underling that even if the two isolators have equal mechanical and geometrical properties, the corresponding normalized friction coefficients (i.e., Eq.s(6f,g)) are different since they refer to different sliding velocities during the

Table 4
Set of near-fault records.

Earthquake	Date	M	Site	Epic. Dist. (km)	Comp.	PGA (g)	PGV (m/s)	PGA(g)/PGV (s/m)	Soil
Imperial Valley-06	1979	6.53	Subway Terminal, L.A.	7.31	SN	0.180	0.545	0.33	C
Imperial Valley-06	1979	6.53	Subway Terminal, L.A.	0.07	SN	0.378	1.150	0.33	C
Imperial Valley-06	1979	6.53	El Centro	7.05	SN	0.357	0.779	0.46	C
Imperial Valley-06	1979	6.53	El Centro	3.95	SN	0.375	0.915	0.41	C
Imperial Valley-06	1979	6.53	El Centro	1.35	SN	0.442	1.119	0.39	C
Imperial Valley-06	1979	6.53	El Centro	0.56	SN	0.462	1.088	0.42	C
Imperial Valley-06	1979	6.53	El Centro	3.86	SN	0.468	0.486	0.96	C
Imperial Valley-06	1979	6.53	El Centro	5.09	SN	0.417	0.596	0.70	C
Morgan Hill	1984	6.19	El Centro	0.53	SN	0.814	0.623	1.31	B
Loma Prieta	1989	6.93	El Centro	9.96	SN	0.294	0.308	0.95	B
Loma Prieta	1989	6.93	El Centro	3.88	SN	0.944	0.970	0.97	B
Landers	1992	7.28	El Centro	2.19	SN	0.704	1.406	0.50	B
Landers	1992	7.28	El Centro	23.62	SN	0.236	0.566	0.42	C
Northridge-01	1994	6.69	El Centro	5.43	SN	0.617	0.674	0.92	B
Northridge-01	1994	6.69	El Centro	5.43	SN	0.518	0.674	0.77	B
Northridge-01	1994	6.69	El Centro	5.92	SN	0.724	1.203	0.60	C
Northridge-01	1994	6.69	El Centro	5.48	SN	0.426	0.878	0.49	C
Northridge-01	1994	6.69	El Centro	6.5	SN	0.870	1.672	0.52	C
Northridge-01	1994	6.69	El Centro	5.35	SN	0.594	1.303	0.46	C
Northridge-01	1994	6.69	El Centro	5.19	SN	0.828	1.136	0.73	B
Northridge-01	1994	6.69	El Centro	5.30	SN	0.733	1.227	0.60	B
Kobe, Japan	1995	6.9	El Centro	0.96	SN	0.854	0.963	0.89	C
Kobe, Japan	1995	6.9	El Centro	0.27	SN	0.645	0.726	0.89	C
Kocaeli, Turkey	1999	7.51	El Centro	10.92	SN	0.241	0.512	0.47	B
Chi-Chi, Taiwan	1999	7.62	El Centro	3.14	SN	0.664	0.777	0.85	B
Chi-Chi, Taiwan	1999	7.62	El Centro	9.96	SN	0.383	0.753	0.51	C
Chi-Chi, Taiwan	1999	7.62	El Centro	3.78	SN	0.286	0.461	0.62	B
Chi-Chi, Taiwan	1999	7.62	El Centro	0.66	SN	0.375	1.655	0.23	B
Chi-Chi, Taiwan	1999	7.62	El Centro	5.97	SN	0.224	0.409	0.55	B
Chi-Chi, Taiwan	1999	7.62	El Centro	5.30	SN	0.157	0.604	0.26	B
Chi-Chi, Taiwan	1999	7.62	3470 WilshireBlvd., L.A.	0.32	SN	0.564	1.846	0.31	B
Chi-Chi, Taiwan	1999	7.62	4680 WilshireBlvd., L.A.	0.91	SN	0.331	0.886	0.37	B
Chi-Chi, Taiwan	1999	7.62	445 Figueroa St., L.A.	2.76	SN	0.310	0.678	0.46	B
Chi-Chi, Taiwan	1999	7.62	Hollywood Storage L.A.	5.18	SN	0.235	0.578	0.41	B
Chi-Chi, Taiwan	1999	7.62	Muroran Harbor	7.00	SN	0.127	0.437	0.29	B
Chi-Chi, Taiwan	1999	7.62	Kushiro Central Wharf	2.13	SN	0.212	0.684	0.31	C
Chi-Chi, Taiwan	1999	7.62	Zihuatenejo, Guerrero Array	1.51	SN	0.295	1.090	0.27	B
Chi-Chi, Taiwan	1999	7.62	Teacalco, Cuerrero Array	6.10	SN	0.133	0.621	0.21	B
Chi-Chi, Taiwan	1999	7.62	Teacalco, Cuerrero Array	9.35	SN	0.224	0.424	0.53	B
Chi-Chi, Taiwan	1999	7.62	Mesa VibradoraC.U., Mexico City	9.96	SN	0.303	0.676	0.45	C

dynamic response. For this reason, each one is used in its peak stead, as follows: $\Pi_{\mu}^{*} = \Pi_{\mu,a}^{*} = \Pi_{\mu,p}^{*} = f_{\max} g/a_0$.

3. Different sets of the seismic inputs

According to the Performance-Based Earthquake Engineering (PBEE) approach [45,46], the performance of the structural system has to be predicted accounting for a wide range of possible ground motions. To this goal, the seismic input is herein given by the product of an intensity measure (IM) denoted as a_0 and a nondimensional function $\ell(\tau)$, such that the uncertainties of the seismic intensity are separated from those related to the characteristics of the record (i.e., record-to-record variability in addition to the event-to-event variability). In this context, the choice of the IM is important to respect the criteria of efficiency, sufficiency and hazard compatibility in agreement with [47–49].

In this study, the *PGA* has been selected as seismic intensity measure a_0 to achieve results useful in any site of the world where the seismic design is based on elastic pseudo-acceleration spectra according to the codes.

It is worthy to highlight that the time scale, adopted in the proposed non-dimensionalization, is the inverse of the ratio $\omega_g = PGA/\ PGV$ and this ratio has been considered efficient in describing the effects of the seismic input on the isolation effectiveness [33–36] and also in being representative of the ground motion characteristics in terms of frequency content [50–54].

For the purposes of this work, a group of 85 non-frequent natural ground motions has been selected, divided into two sets: the first set is made of 45 far-field (FF) records (Tables 1–3) [51] and the second one is composed of 40 near-fault (NF) inputs (Table 4) [55].

In detail, the set of the FF records is divided into three subsets with 15 records, depending on the value of the *PGA*/*PGV* ratio: high ratio (*PGA(g)/PGV* > *1.2* s/m), medium ratio (*0.8* s/m < *PGA(g)/PGV*<*1.2* s/m) and low ratio (*PGA(g)/PGV*<*0.8* s/m).

The NF records of the second set have a low *PGA(g)/PGV* ratio, i.e., on average lower than *0.8* s/m.

In general, high *PGA/PGV* ratios are associated to seismic inputs of short durations and containing high energy content in the low period range while those with low *PGA/PGV* ratios are pulse-type motions with longer durations and contain high energy content in the high period range [50,51,56]. It is noteworthy that, as underlined in Ref. [33], the normalized response of the same system subjected to a seismic input having the same *PGA/PGV* ratio is different, even if the response is normalized with respect to a time scale equal to $1/\omega_g$. This happens because although the ratio *PGA/PGV* is a very effective parameter in providing information on the frequency content and duration of ground motions [33,50,51], it is not completely representative of the ground motion input. It follows the importance to consider a wide set of natural records.

4. Deterministic parameters

The seismic performance of multi-span continuous composite or RC deck bridges isolated with FPS devices is evaluated by considering different ranges of the structural parameters relevant to the problem

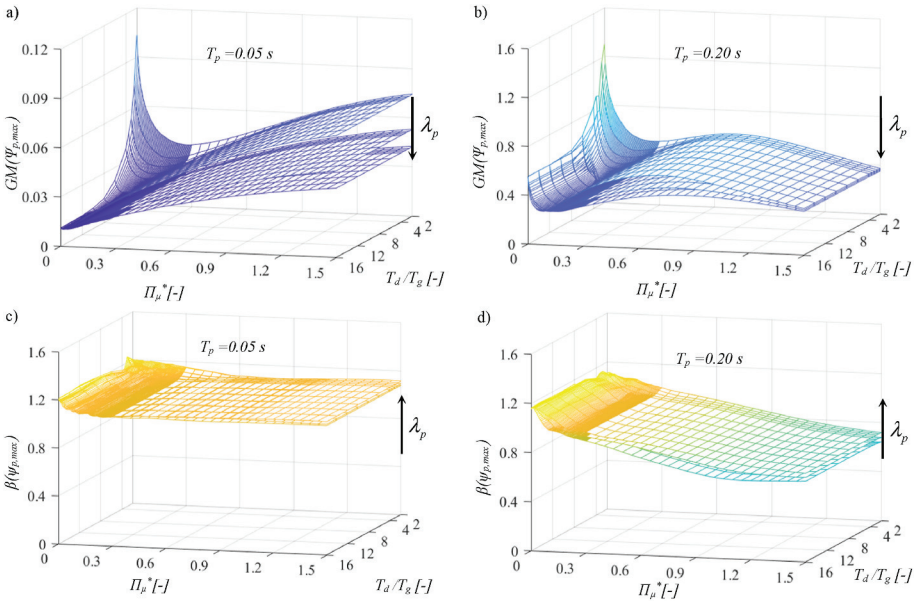

Fig. 2. Geometric mean (a,b) and dispersion (c,d) of the peak nondimensional displacement of the pier top for all the FF records (the arrow indicates the increasing direction of $\lambda_p = 0.1, 0.15, 0.2$).

(introduced in Section 2), according to Refs. [56–58]. Specifically, 4 values of the pier period: $T_p = [0.05, 0.1, 0.15, 0.2]$ s, 11 values of the period ratio: $T_d/T_g = [2, 2.5, 3, 3.5, 4, 6, 8, 10, 12, 14, 16]$; 3 values of the mass ratio: $\Pi_\lambda = [0.1, 0.15, 0.2]$; 85 values of the normalized friction coefficient corresponding to its peak: $\Pi_\mu^* = [0–1.5]$ with a smaller step for values lower than 0.3. Furthermore, the normalized viscous damping factors inherent to the isolator and to the pier are set, respectively, equal to $\Pi_{\xi_d} = 0\%$ and $\Pi_{\xi_p} = 5\%$.

By combining all these structural parameters, a total number of 11200 different bridge models is obtained. Then, solving each structural model for the 85 ground motions, 952000 non-linear dynamic analyses have been carried out. The equations of motion in non-dimensional form (i.e., Eq.s(5a-f)) have been solved in Matlab–Simulink, adopting the ode3 (Bogacki-Shampine) solver [59].

The response parameters (i.e., engineering demand parameters - EDPs) computed with respect to ground in order to evaluate the seismic performance of the bridge models are the peak isolator displacement in its normalized value $\psi_{d,\max} = \frac{u_{d,\max}\omega_g^2}{a_0}$ and the peak pier displacement in its normalized value $\psi_{p,\max} = \frac{u_{p,\max}\omega_g^2}{a_0} = \frac{\left|\left(\sum_{i=1}^{5} u_{pi}\right)\right|_{\max}\omega_g^2}{a_0}$. The former displacements are necessary for the design of the FPS devices and of the seismic deck-abutment joints, while the latter are important to evaluate the internal forces of the substructure (i.e., pier). According to Ref. [30], the response parameters are assumed to follow a lognormal distribution and can be probabilistically treated. Particularly, it can be computed the geometric mean GM together with the dispersion β of the generic response parameter D (i.e., $\psi_{d,\max}$ and $\psi_{p,\max}$) as follows:

$$GM(D) = \sqrt[N]{d_1 \cdot \ldots \cdot d_N} \tag{7}$$

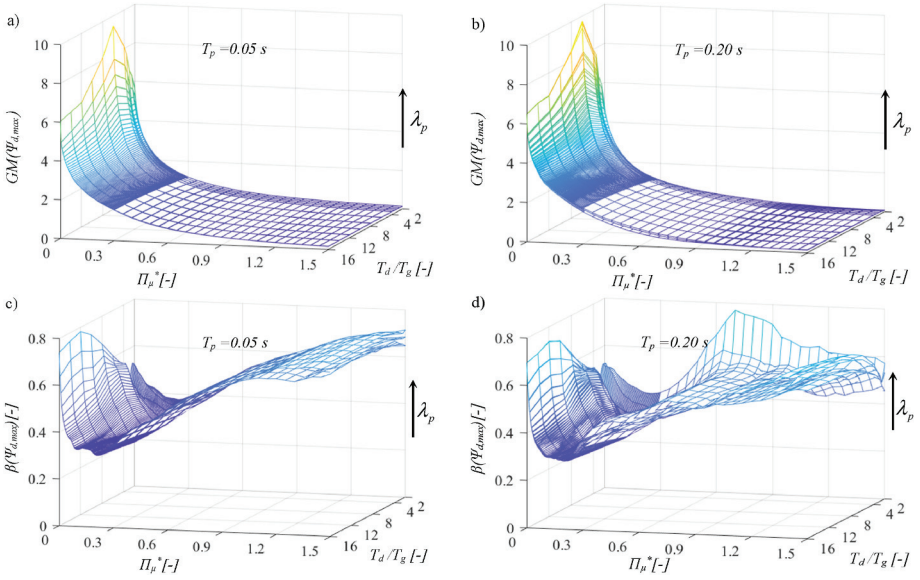

Fig. 3. Geometric mean (a,b) and dispersion (c,d) of the peak nondimensional displacement of the isolation level for all the FF records (the arrow indicates the increasing direction of $\lambda_p = 0.1, 0.15, 0.2$).

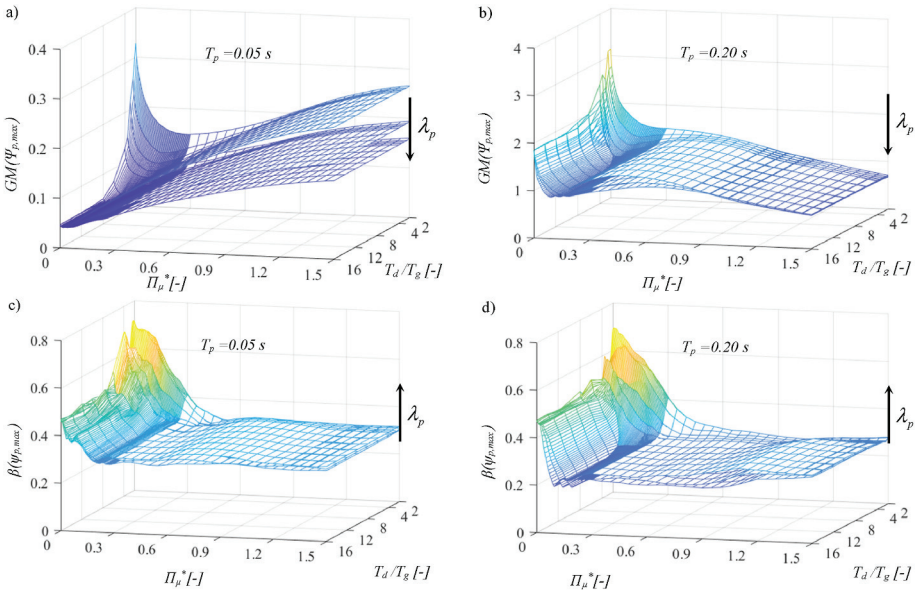

Fig. 4. Geometric mean (a,b) and dispersion (c,d) of the peak nondimensional displacement of the pier top for the FF records with high *PGA(g)/PGV* ratio >1.2 s/m (the arrow indicates the increasing direction of $\lambda_p = 0.1, 0.15, 0.2$).

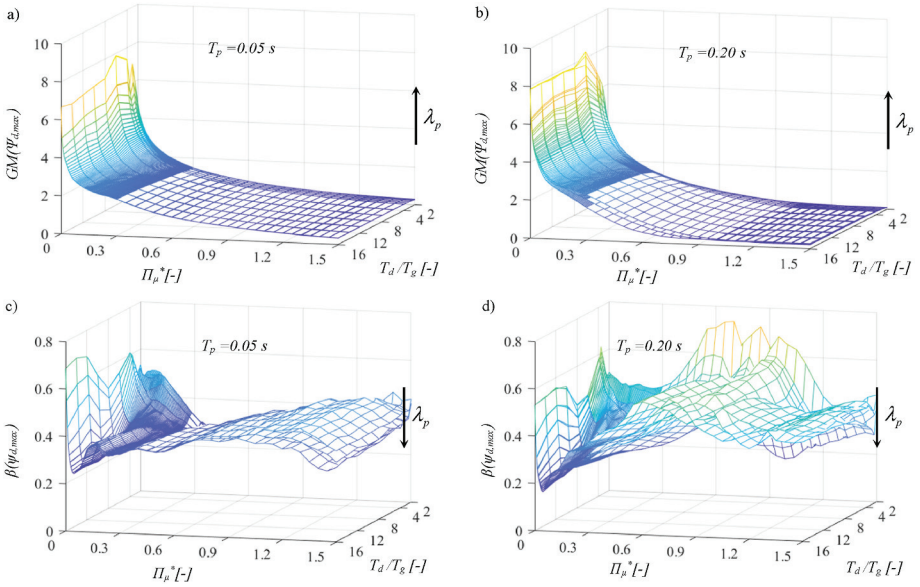

Fig. 5. Geometric mean (a,b) and dispersion (c,d) of the peak nondimensional displacement of the isolation level for the FF records with high *PGA(g)/PGV* ratio >1.2 s/m (the arrow indicates the increasing direction of $\lambda_p = 0.1, 0.15, 0.2$).

$$\beta(D) = \sigma_{ln}(D)\sqrt{\frac{(ln\ d_1 - ln[GM(D)\,])^2 + \ldots\ldots + (ln\ d_N - ln[GM(D)\,])^2}{N-1}} \tag{8}$$

in which d_j is the j-th sample realization of D, and N represents the total number of samples (i.e., earthquake records). Then, the k-th percentile of the response parameter D is computed as:

$$d_k = GM(D)exp[f(k)\beta(D)] \tag{9}$$

where $f(k)$ is equal to 0, 1 and −1 for k equal to the 50th, 16th and 84th percentile, respectively [60]. The lognormality assumption permits to estimate, with a limited number of samples, the response at different percentile levels, which is very useful for system reliability assessment and seismic risk analysis [61].

5. Numerical results

This section illustrates the nondimensional response parameters $\psi_{d,max}$ and $\psi_{p,max}$ in terms of geometric mean and dispersion, as a function of both the peak value of the normalized friction coefficient Π_μ^* and the ratio between the deck and the ground motion period T_d/T_g, for some pier fundamental periods (i.e., $T_p = 0.05$ and 0.2 s) and mass ratios ($\lambda_p = 0.1$, 0.15 and 0.2).

Initially, the results obtained for the first set of the FF records are described. In detail, Fig. 2, Fig. 4, Fig. 6, Fig. 8 regard the normalized pier response $\psi_{p,max}$ for the all FF records, FF records with high *PGA/PGV* ratio, FF records with medium *PGA/PGV* ratio and FF records with low *PGA/PGV* ratio, respectively. In general, $GM(\psi_{p,max})$ increases for lower values of T_d/T_g, especially, for low Π_μ^*.

This happens because the lower is the period of the deck with respect

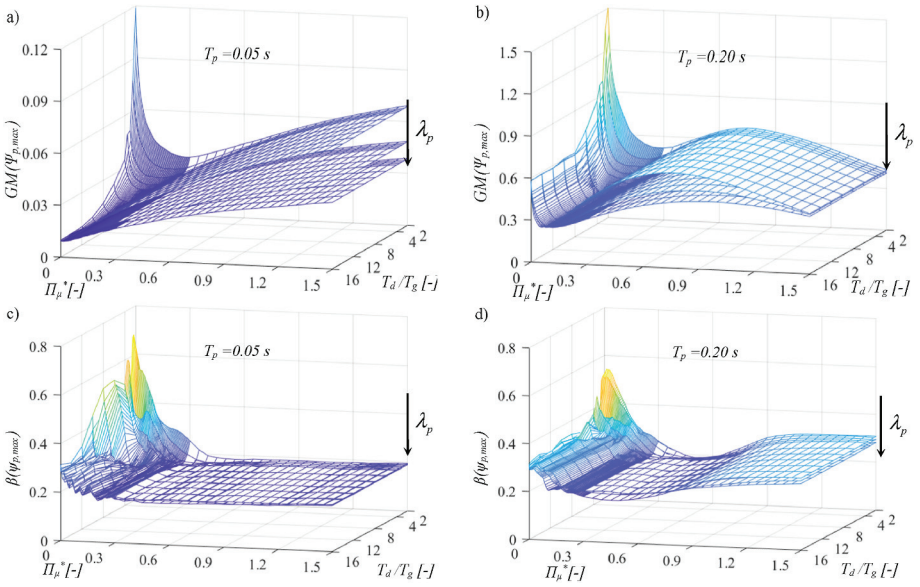

Fig. 6. Geometric mean (a,b) and dispersion (c,d) of the peak nondimensional displacement of the pier top for the FF records with medium *PGA(g)/PGV* ratio in the range 0.8 s/m −1.2 s/m (the arrow indicates the increasing direction of λ_p = 0.1, 0.15, 0.2).

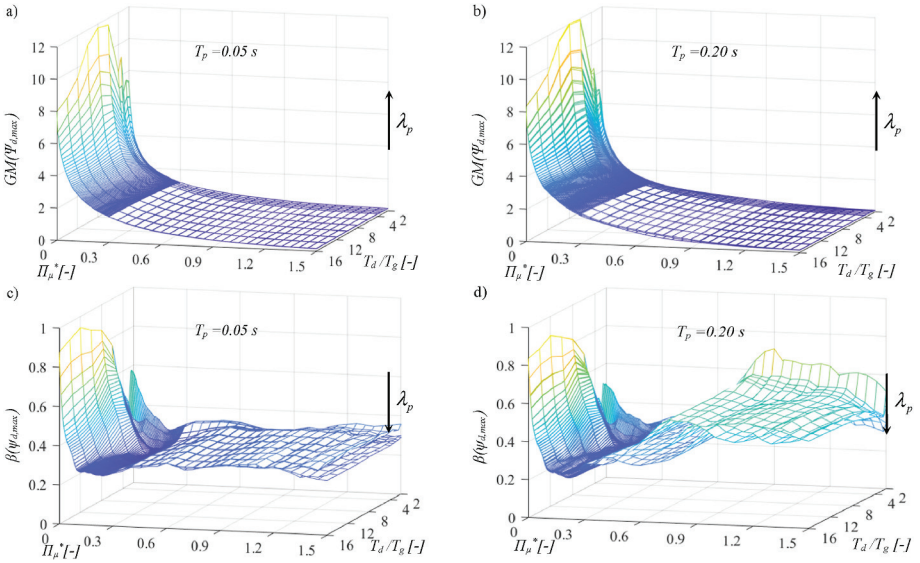

Fig. 7. Geometric mean (a,b) and dispersion (c,d) of the peak nondimensional displacement of the isolation level for the FF records with medium *PGA(g)/PGV* ratio in the range 0.8 s/m −1.2 s/m (the arrow indicates the increasing direction of λ_p = 0.1, 0.15, 0.2).

to the ground motion period, the larger are the forces acting on the deck and thus transmitted to the pier. In addition, $GM(\psi_{p,\max})$ increases for higher values of T_p whereas decreases for larger values of λ_p, since this growth causes a decrease in the forces transmitted from the deck to the pier. However, the influence of the mass ratio is remarkable, especially, for low pier periods. Furthermore, there is a decrease followed by an increase in the response for increasing Π_μ^* values. This leads to highlight the existence of minimal values of $GM(\psi_{p,\max})$ for specific values of Π_μ^*, as also observed in Refs. [29–31].

The analysis of minimal values of $GM(\psi_{p,\max})$ for low Π_μ^* values is better explained in the next section. The response of the pier follows a trend that is similar in all the figures related to the different *PGA/PGV* ratios. The only difference is in the orders of magnitude, since large *PGA/PGV* ratios imply larger pier responses. In this last case and for high T_p values with very low T_d/T_g, the results show also a reduction of the response for very high values of Π_μ^*. The similarity in the trends of the results indicates that for a given combination of the structural parameters, the trends of the median responses are statistically not different if different *PGA/PGV* ratios are considered, confirming that the record selection does not strongly influence the response if $1/\omega_g$ is adopted as the time scale for the normalization [33]. As for the dispersion, $\beta(\psi_{p,\max})$, in general, decreases for higher values of Π_μ^*, remains almost constant for varying values of T_d/T_g and slightly increases for higher values of λ_p.

Fig. 3, Fig. 5, Fig. 7, Fig. 9 show the normalized deck response $\psi_{d,\max}$ for the all FF inputs and for three subsets of the FF records considered. It can be observed slight differences depending on the record selection also regarding the order of magnitude. The values of $GM(\psi_{d,\max})$ first increase with T_d/T_g and then decrease, especially, for low Π_μ^*. This trend is similar to the displacement response spectrum of an isolated mass with a low damping factor. Higher isolated deck periods improve the effectiveness of the isolation. In addition, $GM(\psi_{d,\max})$ is mainly influenced by Π_μ^* since

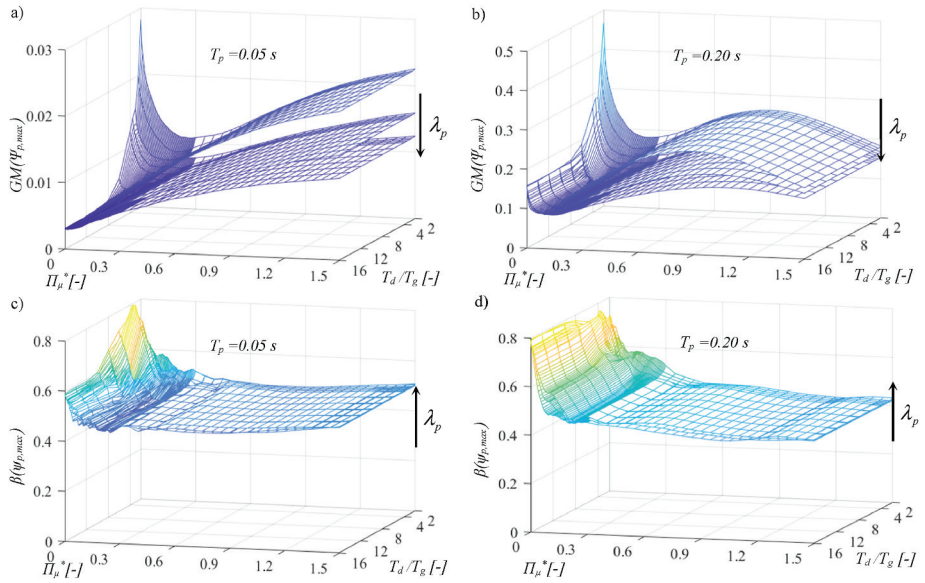

Fig. 8. Geometric mean (a,b) and dispersion (c,d) of the peak nondimensional displacement of the pier top for the FF records with low *PGA(g)/PGV* ratio <0.8 s/m (the arrow indicates the increasing direction of $\lambda_p = 0.1, 0.15, 0.2$).

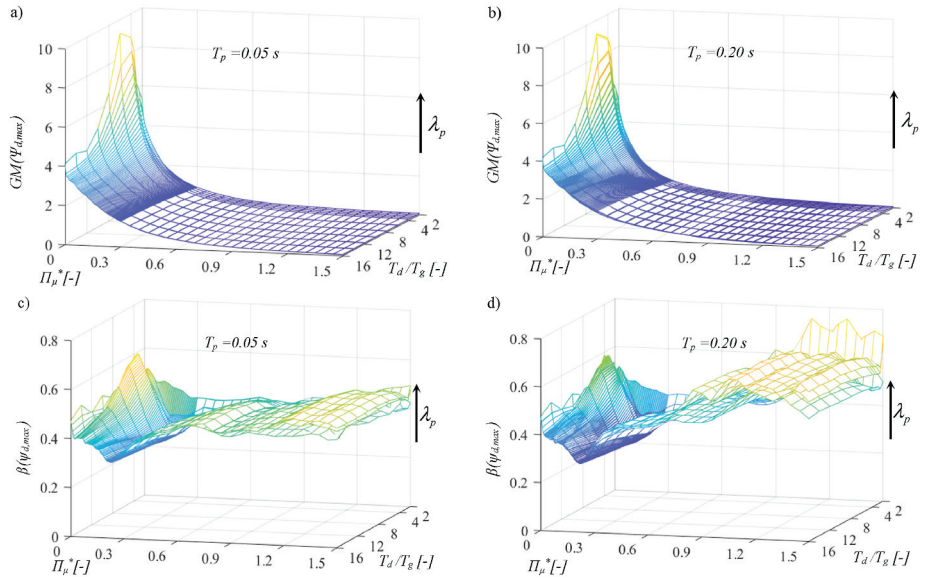

Fig. 9. Geometric mean (a,b) and dispersion (c,d) of the peak nondimensional displacement of the isolation level for the FF records with low *PGA(g)/PGV* ratio <0.8 s/m (the arrow indicates the increasing direction of $\lambda_p = 0.1, 0.15, 0.2$).

the response decreases if this parameter increases due to the energy dissipation showing an hyperbolic trend as obtained in Ref. [30]. Regarding the dispersion, $\beta(\psi_{d,\max})$ is in general quite low, especially, in correspondence of the optimal friction coefficient values minimizing $GM(\psi_{p,\max})$ and strongly increases moving far from these values, since high-linearities are involved.

Similar results (i.e., *GM* and β of both $\psi_{p,\max}$ and $\psi_{d,\max}$) are presented considering the second set related to the NF records and, finally, to the two sets of NF and FF records considered together. Specifically, Figs. 10 and 12 illustrate the statistics of the pier top while Figs. 11 and 13 regard the isolation level. The trend of the responses both in terms of geometric mean and dispersion are very similar to the one obtained by considering the FF records, confirming that the choice of $\omega_g = PGA/PGV$ as the inverse of the time scale is a good indicator of the frequency content of the seismic input. The difference is in the order of magnitude. In fact, the responses of both pier top and isolation system are larger if the FF records are considered. This can appear in contrast with other studies [34–36,62,63] that demonstrate how the NF records are more demanding since characterized by larger dominant pulses. On the other hand, the cyclic characteristic of the larger excitations in case of the FF inputs lead to larger displacement responses as also observed in Refs. [33,56].

From the results, it is noteworthy that Fig. 12(b) shows a reduction of the pier response for very high values of Π_μ^* combined with high T_p values and very low T_d/T_g as also noted in Fig. 2(b) and Fig. 4(b). This is due to the larger dissipation capacity given by the isolators. However, these high values of Π_μ^* lead also to very high dispersions of the isolation response. For this reason combined with the current FPS technology, the search of the optimal parameter Π_μ^* is focused in the range 0–0.5 in the following section.

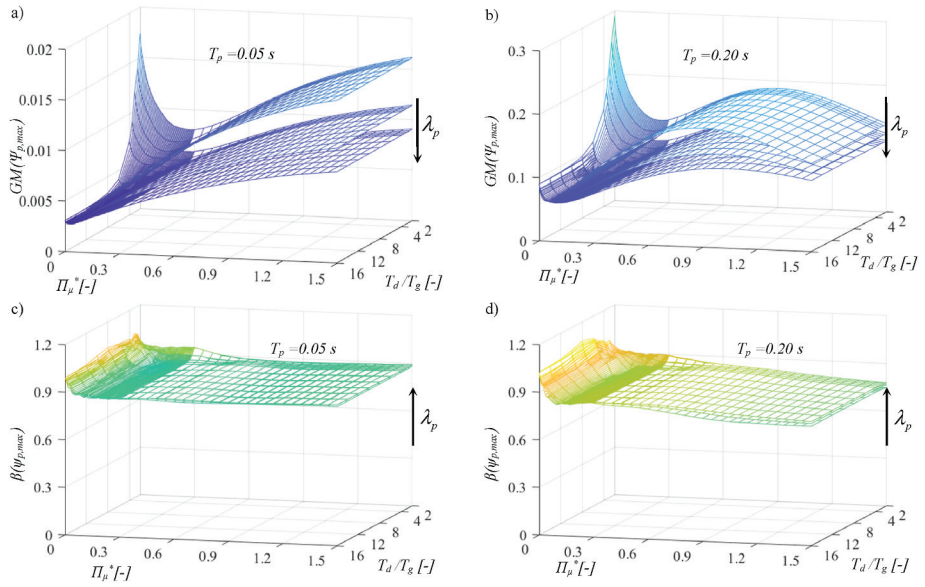

Fig. 10. Geometric mean (a,b) and dispersion (c,d) of the peak nondimensional displacement of the pier top for the NF records (the arrow indicates the increasing direction of $\lambda_p = 0.1, 0.15, 0.2$).

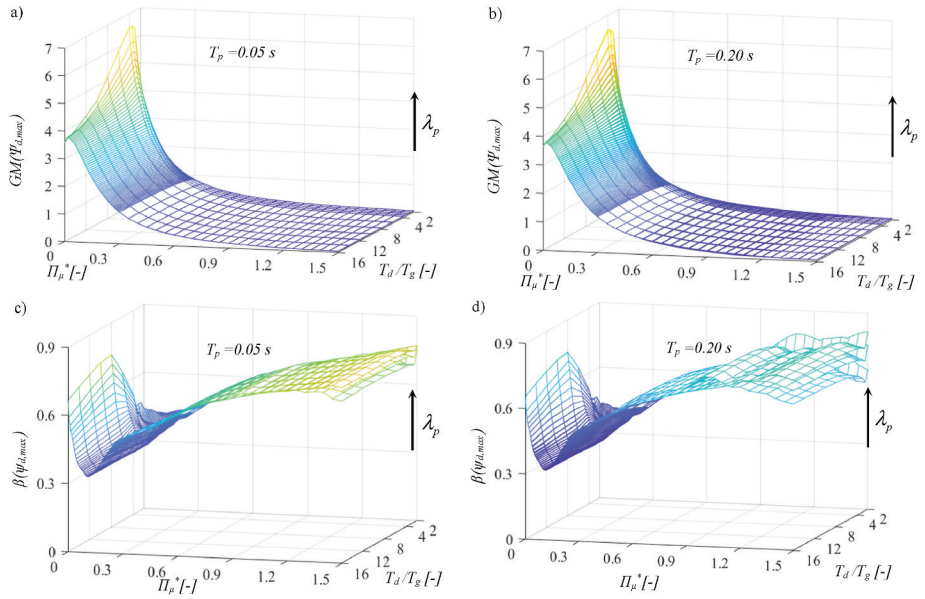

Fig. 11. Geometric mean (a,b) and dispersion (c,d) of the peak nondimensional displacement of the isolation level for the NF records (the arrow indicates the increasing direction of $\lambda_p = 0.1, 0.15, 0.2$).

6. Optimal sliding friction coefficients

As already mentioned, the previous results indicate how it is possible to minimize the normalized response of the pier top for an optimal value of the normalized friction coefficient, denoted as $\Pi^*_{\mu,opt}$.

The existence of this optimum value, deeply discussed in literature [27,28,35,64,65], derives from the equilibrium between two counteracting results caused by increasing Π^*_μ values: on the one hand, there is an increase of the substructure response because higher modes participate and also due to the increase of the isolator strength, determining higher equivalent stiffness [29] of the isolation system, and, thus of the forces transmitted to the pier; on the other hand, the substructure response decreases due to a larger energy dissipation.

Figs. 14 and 15 show the geometric mean of the peak normalized pier response as a function of the normalized friction coefficient for fixed values of the other structural parameters (i.e., T_d/T_g, λ_p and T_p). These figures confirm the observations explained in the previous section with respect to the influence of the *PGA/PGV* ratio values on the pier response. Moreover, as emphasized at the end of the previous section, the maximum normalized value of Π^*_μ assumed to search $\Pi^*_{\mu,opt}$ is set equal to 0.5. From the results, it is possible to observe that the orders of magnitude of the response parameter are different, as previously explained, but the optimum value of the normalized friction coefficient $\Pi^*_{\mu,opt}$ is essentially equal for all the sets and subsets of the records considered, demonstrating the effectiveness of the parameter $\omega_g = PGA/PGV$ within the proposed nondimensional approach. For this reason, the FF and NF records can be considered together in the following.

In Fig. 16, Figs. 17 and 18, it is shown the optimum normalized friction coefficient $\Pi^*_{\mu,opt}$ as a function of the ratio T_d/T_g, for the four different values of the pier period (i.e., $T_p = 0.05, 0.10, 0.15, 0.20$ s) and

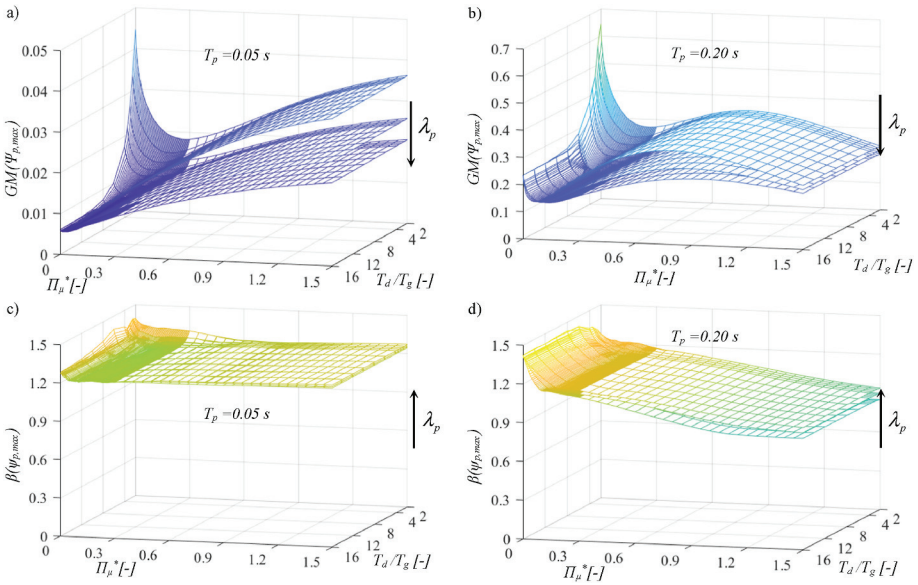

Fig. 12. Geometric mean (a,b) and dispersion (c,d) of the peak nondimensional displacement of the pier top for both the NF and FF records (the arrow indicates the increasing direction of λ_p = 0.1, 0.15, 0.2).

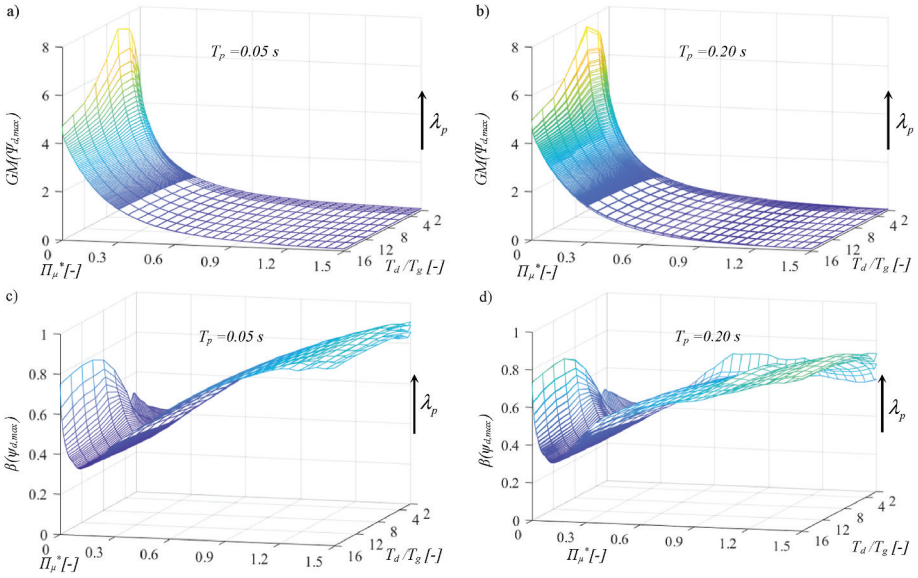

Fig. 13. Geometric mean (a,b) and dispersion (c,d) of the peak nondimensional displacement of the isolation level for both the NF and FF records (the arrow indicates the increasing direction of λ_p = 0.1, 0.15, 0.2).

the three different values of the mass ratio (i.e., λ_p = 0.1, 0.15, 0.2). Specifically, the results are presented considering both the FF and NF records with respect to the 50th, 84th and 16th percentiles, respectively. The optimum normalized friction coefficient decreases with larger T_d/T_g ratios, since the normalized response of the substructure is lower as a consequence of the isolation effectiveness.

Moreover, the values assumed by $\Pi^*_{\mu,opt}$ do not change significantly with the pier period or mass ratio for each percentile. Therefore, the results suggest the possibility of identifying a relationship between $\Pi^*_{\mu,opt}$ and T_d/T_g without considering the other structural parameters, accounting for the 16th, 50th and 84th percentiles.

Thus, the linear regression expression in Eq. (10) has been defined as follows:

$$\Pi^*_{\mu,opt} = a_1 + a_2\Pi_{\omega_g} \tag{10}$$

where the coefficients a_1 and a_2 together with the *R-squared* parameter (Table 5) are evaluated in Matlab [59]. High R-squared values (i.e., close to 1) are obtained, indicating the effectiveness of the formula in computing the optimum normalized friction coefficient. The graphical representation of the proposed linear regression formula is presented in Fig. 19 depending on $T_d/T_g = 1/\Pi_{\omega_g}$.

In this way, knowing the seismic hazard of the site (i.e., knowing *PGA* and *PGV*) and defined the safety level (i.e., the percentile), $\Pi^*_{\mu,opt}$ can be computed through Eq. (10). Then, this result can be used to define the optimal friction coefficient at large velocities of the FPS devices to improve the seismic performance of an isolated multi-span continuous composite or RC deck bridge, through Eq. (11), according to the proposed nondimensionalization:

$$f_{\max,opt} = \Pi^*_{\mu,opt} PGA \Big/ g \tag{11}$$

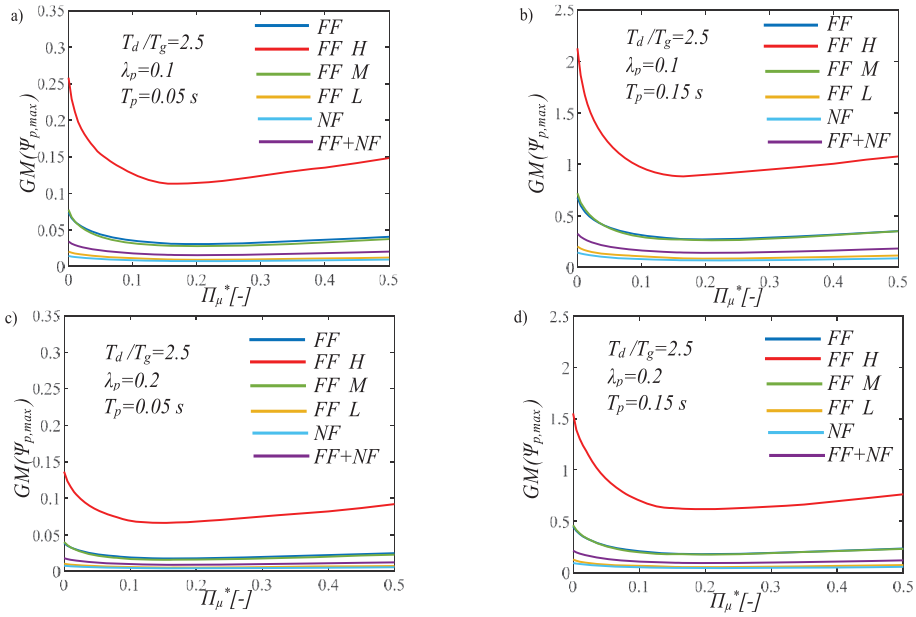

Fig. 14. Geometric mean of the normalized response of the pier top with respect to Π_μ^* for the two sets of records, for $T_d/T_g = 2.5$ and for: a) $\lambda_p = 0.1$ and $T_p = 0.05$ s; b) $\lambda_p = 0.1$ and $T_p = 0.15$ s; c) $\lambda_p = 0.2$ and $T_p = 0.05$ s; d) $\lambda_p = 0.2$ and $T_p = 0.15$ s.

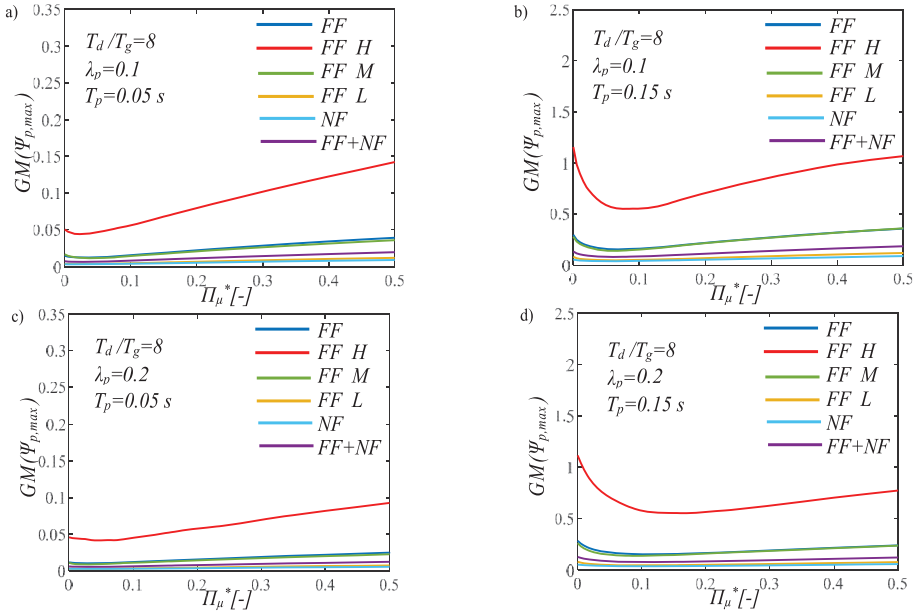

Fig. 15. Geometric mean of the normalized response of the pier top with respect to Π_μ^* for the two sets of records, for $T_d/T_g = 8$ and for: a) $\lambda_p = 0.1$ and $T_p = 0.05$ s; b) $\lambda_p = 0.1$ and $T_p = 0.15$ s; c) $\lambda_p = 0.2$ and $T_p = 0.05$ s; d) $\lambda_p = 0.2$ and $T_p = 0.15$ s.

Regarding the dimensions in plan of the FPS bearings as well as of the abutment-deck joints, the results illustrated in Fig. 3, Fig. 5, Fig. 7, Fig. 9 can be adopted to define the dimensional displacements.

Furthermore, on the basis of the results described in Section 5, a multivariate nonlinear regression analysis has been performed to compute each percentile of the normalized peak displacement of the pier top as a function of the above optimum normalized friction coefficient and of the other structural properties, as follows:

$$\psi_{p,\max}\left(\Pi^*_{\mu,opt}\right) = c_1 + c_2\Pi_g + c_3\Pi_p + c_4\Pi_\lambda + c_5\Pi_g\Pi_p + c_6\Pi_g\Pi_{\lambda_p} + c_7\Pi_p\Pi_\lambda + c_8\Pi_g^2 + c_9\Pi_p^2 + c_{10}\Pi_\lambda^2 \tag{12}$$

where the regression coefficients c_n ($n = 1, \ldots, 10$) are again obtained via Matlab [59] and are reported in Tables 6–9 for the different sets of records. In fact, differently from the optimal value of the friction coefficient, the normalized pier peak response depends on the selected records, as commented in the previous sections. In general, quite high *R-squared* values are obtained for the 16th, 50th and 84th percentile indicating a good estimation of the normalized peak substructure

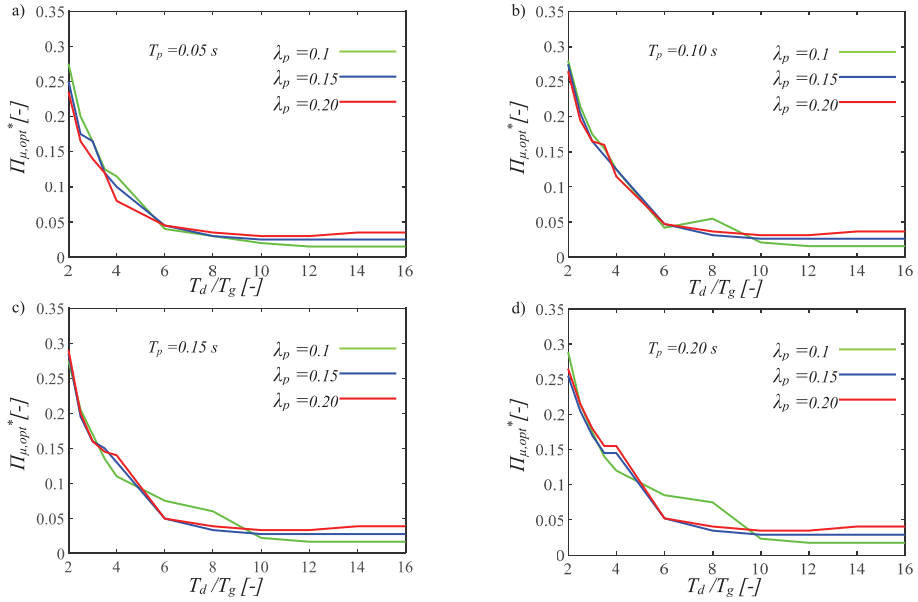

Fig. 16. Optimal values of the normalized friction coefficient minimizing the 50th percentile of substructure response for fixed T_p and varying λ_p, for both the FF and NF records.

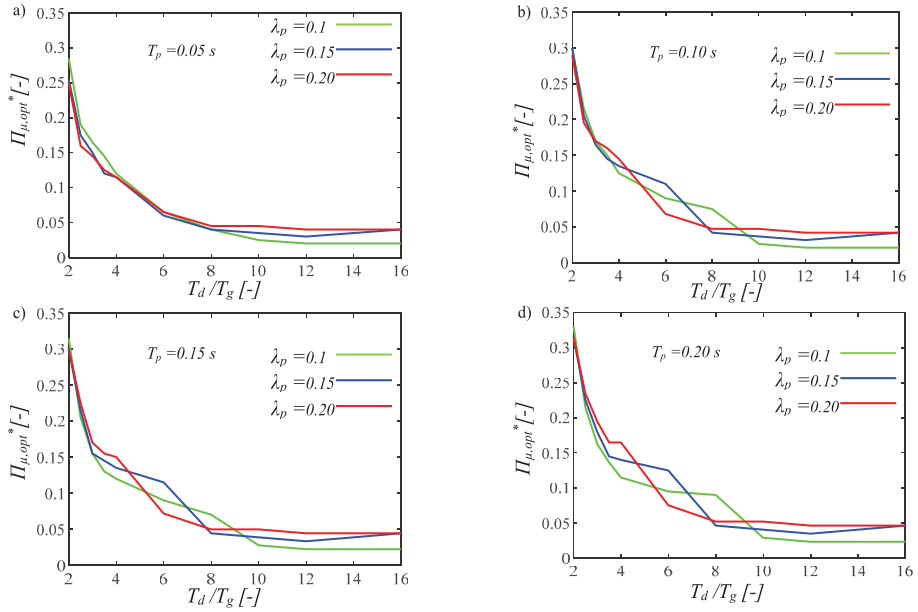

Fig. 17. Optimal values of the normalized friction coefficient minimizing the 84th percentile of substructure response for fixed T_p and varying λ_p, for both the FF and NF records.

response. Similarly to Eq. (11) and according to the non-dimensionalization including the *PGA/PGV* ratio, the results from this regression expression can be achieved in dimensional form as follows:

$$u_{p,\max} = \frac{\psi_{p,\max} PGA}{\omega_g^2} \tag{13}$$

Finally, it is necessary to highlight that the proposed results have been derived assuming only the seismic loads, but during the design or verification of bridges, other serviceability actions, such as thermal movements [66], have to be absolutely considered, especially, when high friction coefficients are required under strong earthquake events. In these cases, a global cost-effectiveness analysis is suggested to reduce the costs if the same safety level is assured. Additionally, for lifetime assessments, the deterioration of the sliding surface of the isolators can be accounted for by means of the property modification factors [67].

7. Conclusions

This work is aimed at evaluating the optimal properties of single concave friction pendulum (FPS) bearings employed for the seismic isolation of multi-span continuous composite or RC deck bridges. The ground motion characteristics have been taken into account by means of both the peak ground acceleration (*PGA*) and parameter T_g expressed as a function of the peak ground acceleration-to-velocity (*PGA/PGV*) ratio

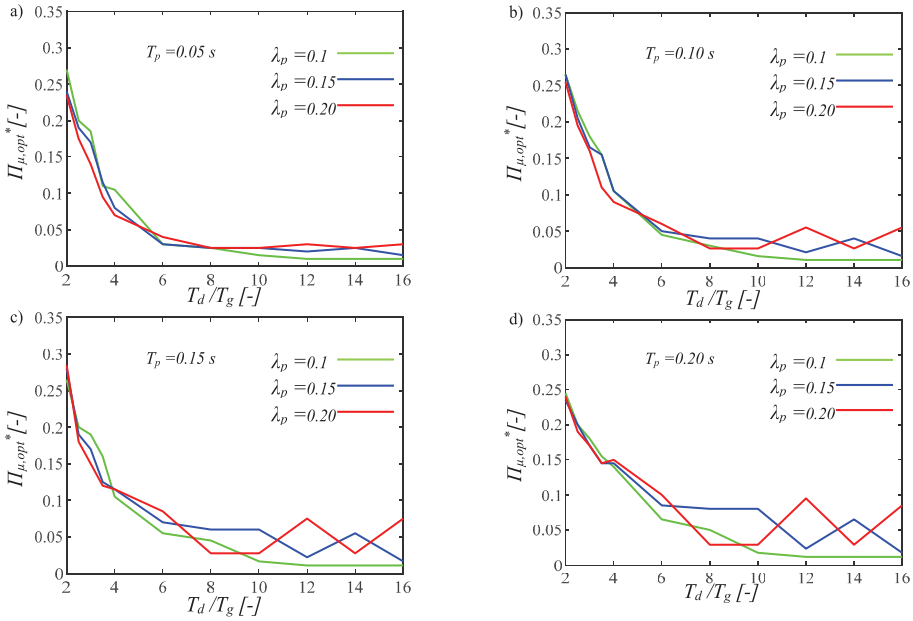

Fig. 18. Optimal values of the normalized friction coefficient minimizing the 16th percentile of substructure response for fixed T_p and varying λ_p, for both the FF and NF records.

Table 5
Linear regression coefficients for the optimum normalized friction coefficient.

	R-squared	a_1	a_2
*16*th	0.9264	−0.0177	0.5374
*50*th	0.9654	−0.0234	0.5699
*84*th	0.9517	−0.0138	0.5774

(i.e., $T_g = 2\pi/\omega_g = 2\pi PGV/PGA$). These parameters have been employed as the length scale and time scale factors to develop a non-dimensional formulation to assess the normalized response of the six-degree-of-freedom structural model under different seismic events. Specifically, two different families of ground motions corresponding to the near-fault and far-field seismic records have been considered. The far-field events have been divided into three subsets depending on the *PGA/PGV* ratio. A wide set of natural records has been selected to take

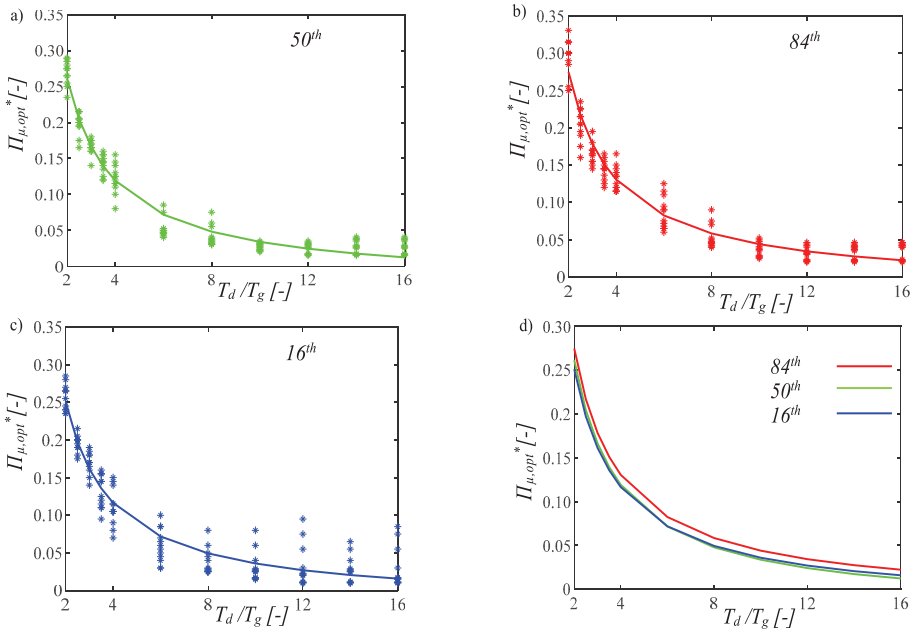

Fig. 19. Regression of the optimum normalized friction coefficient for both the FF and NF records related to a) the 50th percentile, b) the 16th percentile, c) the 84th percentile and d) all the percentiles.

Table 6
Regression coefficients for the normalized peak pier top displacement considering the FF records with high *PGA/PGV* ratio.

	R-squared	c_1	c_2	c_3	c_4	c_5	c_6	c_7	c_8	c_9	c_{10}
*16*th	0.8238	0.0883	−0.0439	4.7266	−1.0243	−0.2112	0.0390	−1.776	0.0026	−7.0046	2.1065
*50*th	0.7805	0.1798	−0.0666	5.3996	−1.0505	−0.2439	0.0178	4.1849	0.0039	−11.743	1.0663
*84*th	0.7117	0.0268	−0.0704	6.2188	1.4000	−0.2709	−0.0461	8.5401	0.0045	−16.174	−6.2984

Table 7
Regression coefficients for the normalized peak pier top displacement considering the FF records with medium *PGA/PGV* ratio.

	R-squared	c_1	c_2	c_3	c_4	c_5	c_6	c_7	c_8	c_9	c_{10}
*16*th	0.8838	0.0345	−0.0103	1.5704	−0.6654	−0.1352	0.0259	−2.4860	0.0008	2.5288	1.8654
*50*th	0.9155	0.0559	−0.0150	2.1355	−0.9729	−0.1850	0.0352	−3.0752	0.0011	3.1803	2.6501
*84*th	0.9302	0.0312	−0.0025	2.6361	−1.3887	−0.2381	0.0412	−4.5669	0.0005	5.8894	4.1816

Table 8
Regression coefficients for the normalized peak pier top displacement considering the FF records with low *PGA/PGV* ratio.

	R-squared	c_1	c_2	c_3	c_4	c_5	c_6	c_7	c_8	c_9	c_{10}
*16*th	0.9094	0.0245	−0.0030	0.4780	−0.4384	−0.0327	0.0002	−2.0052	0.0003	1.2832	1.8503
*50*th	0.9089	0.0194	−0.0096	0.7360	−0.1434	−0.0680	0.0228	−1.8481	0.0006	1.6322	0.2305
*84*th	0.9016	0.0259	−0.0078	1.2774	−0.5507	−0.1050	0.0195	−3.8552	0.0006	2.9155	2.0023

Table 9
Regression coefficients for the normalized peak pier top displacement considering the NF records.

	R-squared	c_1	c_2	c_3	c_4	c_5	c_6	c_7	c_8	c_9	c_{10}
*16*th	0.9256	0.0085	−0.0027	0.0842	−0.0132	−0.011	0.0148	−0.0207	0.0001	0.7299	−0.3325
*50*th	0.9194	−0.0609	−0.0011	0.747	0.5680	−0.0308	−0.007	−3.276	0.0002	1.4395	−1.0878
*84*th	0.8503	0.1372	−0.0185	0.5895	−1.2617	−0.0584	0.0776	0.5413	0.0006	2.7691	2.0480

into account the record-to-record and event-to-event variability with respect to the simplified assumption of T_g. Furthermore, many bridge systems have been analyzed by varying: the pier fundamental period T_p, the ratio between the fundamental period of the isolated deck and the period of the ground motion T_d/T_g, the mass ratio λ_p and the normalized friction coefficient Π_μ^*. The results of the seismic analyses show that:

- the normalized response for both the isolation system and pier is strongly influenced by the ratio T_d/T_g. In detail, by increasing the ratio T_d/T_g, the geometric mean of the isolator normalized response first increases, until reaching a peak, and then decreases following the trend of a displacement response spectrum. On the other hand, the geometric mean of the substructure response decreases for increasing values of T_d/T_g;
- the response for both the substructure and deck follows a very similar trend for the different sets of the records considered (i.e., *PGA/PGV* ratios). Different orders of magnitude are achieved, especially, for the pier response. Particularly, the far-field records, especially, with a high *PGA/PGV* ratio are more demanding since they are characterized by many pulses in a wider range of frequency. The similarity of the trends confirms that the choice of $1/\omega_g$ to define the time scale within the proposed nondimensionalization is very effective;
- the response of the isolation system is not particularly influenced by both the mass ratio and pier period;
- the optimum values of the normalized friction coefficient are defined to minimize the different percentiles of the normalized pier displacement. These optimum values are lower if larger $T_d/\ T_g$ values are considered and are not significantly affected by the other bridge parameters. In addition, the optimal coefficients do not depend on the set of the records considered confirming the effectiveness of the *PGA/PGV* ratio.

All these considerations have led to propose a formula for the design of FPS bearings to calculate the normalized optimum friction coefficient depending only on the T_d/T_g ratio and, thus, on the seismic hazard of the reference site, through a linear regression expression. In addition, a multivariate nonlinear regression analysis is also presented to assess the different percentiles of the pier response, which depend on the T_d/T_g ratio, characteristics of the records set and bridge structural parameters.

Author statement

Castaldo Paolo: Supervision, Visualization, Conceptualization, Methodology, Writing- Reviewing and Editing, Validation, Formal analysis.

Miceli Elena: Supervision, Visualization, Conceptualization, Methodology, Software, Writing- Original draft, Data curation, Writing-Reviewing and Editing, Validation, Investigation, Formal analysis.

Declaration of competing interest

"No conflict of interest."

"The authors declare that they have no known competing financial interests or personal relationships that could have appeared to influence the work reported in this paper."

Data availability

Data will be made available on request.

Acknowledgements

This work is part of the collaborative activity developed by the authors within the framework of the "PNRR": SPOKE 7 "CCAM, Connected Networks and Smart Infrastructure" - WP4.

This study was carried out within the RETURN Extended Partnership (National Recovery and Resilience Plan – NRRP, Mission 4, Component 2, Investment 1.3 – D.D. 1243 2/8/2022, PE0000005).

This work is also part of the collaborative activity developed by the authors within the research project "RELUIS - PONTI".

References

[1] Ghobarah A, Ali HM. Seismic performance of highway bridges. Eng Struct 1988;10.
[2] Tsopelas P, Constantinou MC, Okamoto S, Fujii S, Ozaki D. Experimental study of bridge seismic sliding isolation systems. Eng Struct 1996;18(4):301–10.
[3] Jangid RS. Seismic response of isolated bridges. J Bridge Eng 2004;9(2):156–66.
[4] Constantinou MC, Whittaker AS, Fenz DM, Apostolakis G. Seismic isolation of bridges. Buffalo, NY 14260: Department of Civil, Structural and Environmental Engineering, University at Buffalo, State University of New York; 2007.
[5] Tsiavos A, Alexander NA, Diambra A, Gonzalez-Buelga A, Sextos A. A sand-rubber deformable granular layer as a low-cost seismic isolation strategy in developing countries: experimental investigation. Soil Dynam Earthq Eng 2019;125:105731.
[6] Rele R, Balmukund R, Bhattacharya S, Cui L, Mitoulis SA. Application of controlled-rocking isolation with shape memory alloys for an overpass bridge. Soil Dynam Earthq Eng 2021;149:106827.
[7] Tongaonkar NP, Jangid RS. Seismic response of isolated bridges with soil–structure interaction. Soil Dynam Earthq Eng 2003;23:287–302.
[8] Zayas VA, Low SS, Mahin SA. A simple pendulum technique for achieving seismic isolation. Earthq Spectra 1990;6(2):317–33.
[9] Su L, Ahmadi G, Tadjbakhsh IG. Comparative study of base isolation systems. J Eng Mech 1989;115(9):1976–92.
[10] Mokha A, Constantinou MC, Reinhorn AM. Teflon bearings in base isolation. I: testing. J Struct Eng 1990;116(2):438–54.
[11] Constantinou MC, Mokha A, Reinhorn AM. Teflon bearings in base isolation. II: modeling. J Struct Eng 1990;116(2):455–74.
[12] Almazàn JL, De la Llera JC. Physical model for dynamic analysis of structures with FPS isolators. Earthq Eng Struct Dynam 2003;32(8):1157–84.
[13] Mosqueda G, Whittaker AS, Fenves GL. Characterization and modeling of Friction Pendulum bearings subjected to multiple components of excitation. J Struct Eng 2004;130(3):433–42.
[14] Jangid RS. Computational numerical models for seismic response of structures isolated by sliding systems. Struct Control Health Monit 2005;12:117–37.
[15] Jangid RS. Stochastic response of bridges seismically isolated by friction pendulum system. J Bridge Eng 2008;13(4):319.
[16] Constantinou MC, Whittaker AS, Kalpakidis Y, Fenz DM, Warn GP. Performance of seismic isolation hardware under service and seismic loading. 2007. *Technical Report* MCEER-07-0012.
[17] Bonessio N, Lomiento G, Benzoni G. Damage identification procedure for seismically isolated bridges. Struct Control Health Monit 2012;19:565–78.
[18] Tsiavos A, Vassiliou MF, Mackie KR, Stojadinovic B. Comparison of the inelastic response of base-isolated structures to near-fault and far-fault ground motions. In: VEESD 2013, Vienna congress on recent advances in earthquake engineering and structural dynamics & D-A-CH Tagung; August, 2013. p. 28–30. Vienna, Austria.
[19] Tsiavos A, Schlatter D, Markic T, Stojadinovic B. Experimental and analytical investigation of the inelastic behavior of structures isolated using friction pendulum bearings. Procedia Eng 2017;199:465–70.
[20] Landi L, Grazi G, Diotallevi P. Comparison of different models for friction pendulum isolators in structures subjected to horizontal and vertical ground motions. Soil Dynam Earthq Eng 2016;81:75–83.
[21] Kim Young-Suk, Yun Chung-Bang. Seismic response characteristics of bridges using double concave friction pendulum bearings with tri-linear behaviour. Eng Struct 2007;29:3082–93.
[22] Kunde MC, Jangid RS. Effects of pier and deck flexibility on the seismic response of isolated bridges. J Bridge Eng 2006;11(1):109–21.
[23] Meng Dongliang, Yang Menggang, Yang Ziqi, Chouw Nawawi. Effect of earthquake-induced transverse poundings on a 32 m span railway bridge isolated by friction pendulum bearings. Eng Struct 2022;251:113538.
[24] Eröz M, DesRoches R. The influence of design parameters on the response of bridges seismically isolated with the friction pendulum system (FPS). Eng Struct 2013;56:585–99.
[25] Panchal VR, Jangid RS, Shobhana Bhargav B. Seismic performance of bridges with variable friction pendulum system. Int J Struct Eng 2021;11(4):342–63.
[26] Castaldo P, Amendola G, Giordano L, Miceli E. Seismic reliability assessment of isolated multi-span continuous deck bridges. Ingegneria Sismica - Int J Earthquake Eng 2022. Anno XXXIX – Num. 3.
[27] Jangid RS. Optimum frictional elements in sliding isolation systems. Comput Struct 2000;76(5):651–61. 10.
[28] Jangid RS. Optimum friction pendulum system for near-fault motions. Eng Struct 2005;27(3):349–59.
[29] Castaldo P, Ripani M, Lo Piore R. Influence of soil conditions on the optimal sliding friction coefficient for isolated bridges. Soil Dynam Earthq Eng 2018;111:131–48. https://doi.org/10.1016/j.soildyn.2018.04.056.
[30] Castaldo P, Guglielmo Amendola. Optimal sliding friction coefficients for isolated viaducts and bridges: a comparison study. Struct Control Health Monit 2021;28 (12):e2838. https://doi.org/10.1002/stc.2838.
[31] Castaldo P, Amendola G. Optimal DCFP bearing properties and seismic performance assessment in nondimensional form for isolated bridges. Earthquake Eng Struct Dyn, 2021 2021;50(9):2442–61. https://doi.org/10.1002/eqe.3454.
[32] Tsiavos A, Haladij P, Sextos A, Alexander NA. Analytical investigation of the effect of a deformable sliding layer on the dynamic response of seismically isolated structures. Structures 2020;27:2426–36.
[33] Castaldo P, Tubaldi E. Influence of ground motion characteristics on the optimal single concave sliding bearing properties for base-isolated structures. Soil Dynam Earthq Eng 2018;104:346–64. 1984.
[34] Liao WI, Loh CH, Lee BH. Comparison of dynamic response of isolated and nonisolated continuous girder bridges subjected to near-fault ground motions. Eng Struct 2004;26(14):2173–83.
[35] Dicleli M, Buddaram S. Effect of isolator and ground motion characteristics on the performance of seismic-isolated bridges. Earthq Eng Struct Dynam 2006;35(2): 233–50.
[36] Hameed A, Koo MS, Dai Do T, Jeong JH. Effect of lead rubber bearing characteristics on the response of seismic-isolated bridges. KSCE J Civ Eng 2008;12 (3):187–96.
[37] Olmos BA, Jara JM, Roesset JM. Effects of isolation on the seismic response of bridges designed for two different soil types. Bull EarthEng 2011;9(2):641–56.
[38] Dehghanpoor A, Thambiratnam D, Taciroglu E, Chan T. Soil-pile-superstructure interaction effects in seismically isolated bridges under combined vertical and horizontal strong ground motions. Soil Dynam Earthq Eng 2019;126:105753.
[39] Dehghanpoor A, Thambiratnam D, Zhang W, Chan T, Taciroglu E. An extended probabilistic demand model with optimal intensity measures for seismic performance characterization of isolated bridges under coupled horizontal and vertical motions. Bull Earthq Eng 2021;19(5):2291–323.
[40] Papadopoulos SP, Sextos AG. Anti-symmetric mode excitation and seismic response of base-isolated bridges under asynchronous input motion. Soil Dynam Earthq Eng 2018;113:148–61. https://doi.org/10.1016/j.soildyn.2018.06.004.
[41] Makris N, Black CJ. Dimensional analysis of inelastic structures subjected to near fault ground motions. Berkeley: Earthquake Engineering Research Center, University of California; 2003. Technical report: EERC 2003/05.
[42] Makris N, Black CJ. Dimensional analysis of bilinear oscillators under pulse-type excitations. J Eng Mech 2004;130(9):1019–31.
[43] Barenblatt GI. Scaling, self-similarity, and intermediate asymptotics. Cambridge, U. K: Cambridge University Press; 1996.
[44] Langhaar HL. Dimensional analysis and theory of models. New York: Wiley; 1951.
[45] Aslani H, Miranda E. Probability-based seismic response analysis. Eng Struct 2005; 27(8):1151–63.
[46] Porter KA. An overview of PEER's performance-based earthquake engineering methodology. In: Proceedings, proceedings of the 9th international conference on application of statistics and probability in civil engineering (ICASP9); 2003. San Francisco, California.
[47] Shome N, Cornell CA, Bazzurro P, Carballo JE. Earthquake, records, and nonlinear responses. Earthq Spectra 1998;14(3):469–500.
[48] Pinto PE, Giannini R, Franchin P. Seismic reliability analysis of structures. Pavia, Italy: IUSS Press; 2003.
[49] Luco N, Cornell CA. Structure-specific scalar intensity measures for near-source and ordinary earthquake ground motions. Earthq Spectra 2007;23(2):357–92.
[50] Zhu TJ, Tso WK, Heidebrecht AC. Effect of peak ground A/V ratio on structural damage. J Struct Eng 1988;114:1019–37.
[51] Tso WK, Zhu TJ, Heidebrecht AC. Engineering implication of ground motion A/V ratio. Soil Dynam Earthq Eng 1992;11(3):133–44.
[52] Palermo M, Silvestri S, Gasparini G, Trombetti T. A statistical study on the peak ground parameters and amplification factors for an updated design displacement spectrum and a criterion for the selection of recorded ground motions. Eng Struct 2014;76:163–76.
[53] Sawada T, Hirao K, Yamamoto H, Tsujihara O. Relation between maximum amplitude ratio and spectral parameters of earthquake ground motion. In: Proc. 10th world conf. on earthquake engineering, vol. 2; 1992. p. 617–22.
[54] Pavel F, Lungu D. Correlations between frequency content indicators of strong ground motions and PGV. J Earthq Eng 2013;17(4):543–59.
[55] PEER ground motion database web application beta version. October 1, 2010.
[56] Chopra AK, Chintanapakdee C. Comparing response of SDF systems to near-fault and far-fault earthquake motions in the context of spectral regions. Earthq Eng Struct Dynam 2001;30:1769–89. https://doi.org/10.1002/eqe.92.
[57] P, Palazzo B, Ferrentino T. Seismic reliability-based ductility demand evaluation for inelastic base-isolated structures with friction pendulum devices. Earthq Eng Struct Dynam 2017;46(8):1245–66. https://doi.org/10.1002/eqe.2854.
[58] Ryan K, Chopra A. Estimation of seismic demands on isolators based on nonlinear analysis. J Struct Eng 2004;130(3):392–402.
[59] Math Works Inc. MATLAB-high performance numeric computation and visualization software. MA, USA: User's Guide. Natick; 1997.
[60] Ang AHS, Tang WH. Probability concepts in engineering-emphasis on applications to civil and environmental engineering. New York, USA: John Wiley & Sons; 2007.
[61] Cornell C, Jalayer F, Hamburger R, Foutch D. Probabilistic basis for 2000 SAC Federal Emergency Management Agency steel moment frame guidelines. J Struct Eng 2002;128(4):526–33.
[62] Jangid RS, Kelly JM. Base isolation for near-fault motions. Earthq Eng Struct Dynam 2001;30:691–707.
[63] Mazza F, Vulcano A. Nonlinear response of RC framed buildings with isolation and supplemental damping at the base subjected to near-fault earthquakes. J Earthq Eng 2009;13(5):690–715.
[64] Fragiacomo M, Rajgelj S, Cimadom F. Design of bilinear hysteretic isolation systems. Earthq Eng Struct Dynam 2003;32(9):1333–52.
[65] Iemura H, Taghikhany T, Jain S. Optimum design of resilient sliding isolation system for seismic protection of equipments. Bull Earthq Eng 2007;5(1):85–103.
[66] National Cooperative Highway Research. NCHR program report 276Thermal effects in concrete bridge superstructures. 1985.
[67] Warn Gordon P, Whittaker Andrew S. Property modification factors for seismically isolated bridges. J Bridge Eng 2006;11(3). 1084-0702.